Arch. Mech., 33, 5, pp. 625–661, Warszawa 1981

Asymmetric supercritical flow past a double wedge with embedded shocks

K. S. CHANG and M. HOLT (BERKELEY)

SUPERCRITICAL transonic flow past a double wedge at a small angle of attack is analyzed in the hodograph plane. The flow is treated as steady, two-dimensional and inviscid, and is assumed to be isentropic and irrotational. Along the wedge surface the stagnation points are assumed to be attached at the forward and rear vertices and sonic speed is, a priori, attained at the upper and lower shoulders of the double wedge. The flow is mapped onto a hodograph plane containing two folds of a Riemann surface which are subsequently separated by a cut inserted along a branch line. In each of the two Riemann folds a numerical technique based on Telenin's method and a double sweep method is used to solve the two-boundary value problems, one for the stream function and the other for the velocity potential. The solutions exhibit many-sheeted flows in the physical plane, due to the presence of limit lines on which the Jacobian of the transformation from the hodograph to the physical plane vanishes.

Ponadkrytyczny, okołodźwiękowy opływ klina dwustronnego pod małym kątem natarcia rozważa się w płaszczyźnie hodografu. Przepływ traktuje się jako ustalony, dwuwymiarowy i nielepki i zakłada się również, że jest on izentropowy i bezwirowy. Zakłada się, że punkty spiętrzenia przytwierdzone są do powierzchni klina na krawędziach natarcia i spływu, a prędkość dźwięku osiągana jest *a priori* na górnej i dolnej powierzchni dwustronnego klina. Przepływ odwzorowuje się na płaszczyźnie hodografu zawierającej dwa płaty powierzchni Riemanna, które następnie oddziela się za pomocą rozcięcia wzdłuż linii rozgałęzienia. Na każdym płacie powierzchni Riemanna stosuje się technikę numeryczną opartą na metodzie Telenina oraz metodzie podwójnego przejścia, rozwiązując dwa zagadnienia brzegowe: jedno dla funkcji prądu, a drugie dla potencjału prędkości. Rozwiązania wykazują przepływy wielopowłokowe w płaszczyźnie fizycznej, co wywołane jest obecnością linii granicznych, na których znika jakobian przekształcenia z płaszczyzny hodografu na płaszczyznę fizyczną. Odwzorowanie odwrotne na płaszczyznę fizyczną prowadzi do pola przepływu fizycznego zawierającego parę skośnych fal uderzeniowych.

Сверхкритическое, околозвуковое обтекание двухстороннего клина под малым углом атаки рассматривается в плоскости годографа. Течение трактуется как установившиеся, двухмерное и несжимаемое и предполагается тоже, что является оно изэнтропическим и безвихревым. Предполагается, что критические точки закреплены к поверхности клина на передней и задней гранях, а скорость звука достигается априори на верхней и нижней поверхностях двухстороннего клина. Течение отображается на плоскости годографа, содержавшей два листа римановой поверхности, которые затем разделяется при помощи сечения вдоль линии ветвления. На каждом листе римановой поверхности применяется численная техника опирающаяся на метод Теленина и метод двойного перехода, решая две граничные задачи: одну для функции тока, а вторую для потенциала скорости. Решения указывают на многооболочечные течения в физической плоскости, что вызвано присутствием граничных линий, на которых исчезает якобиан преобразования из плоскости годографа в физическую плоскость. Обратное отображение на физическую плоскость приводит к полю физического течения, содержавшего пару косых ударных волн.

1. Introduction

1.1. Transonic phenomena

THE TERM transonic is used both when a subsonic pocket of flow in a supersonic region is generated downstream of a shock wave and when a local zone of supersonic flow is embedded in a subsonic region. The boundary of the localized zone is, in general, made up of a sonic line, a nozzle or an airfoil surface, and a shock wave. Over the past fifteen years the topic of transonic flow has received renewed attention. Most of the present day civil aircraft fly within the transonic Mach number range. Transition through the sonic range is of critical importance in the design of supersonic aircraft and missiles.

Mathematically, the differential equations governing the transonic flows are of mixed type, changing from elliptic in subsonic regions to hyperbolic in supersonic regions. A theory of linear mixed equations has been developed in the literature; however, for the nonlinear equations which govern the present problem additional difficulties arise. Moreover, discontinuities are, in general, expected in the transonic flow as part of the solution.

1.2. Brief review of the literature

The usual assumption made in attacking problems of steady two-dimensional transonic flows past airfoils with embedded shock waves is that the upstream Mach number is moderate ($M_\infty < 1.3$) so that entropy changes are not significant and a velocity potential can be introduced. The literature in transonic flow either deals with governing equations written directly in physical coordinates, or, if the flow is steady and two-dimensional, with the hodograph equations. In addition, simplified nonlinear transonic equations may be considered basing on the small perturbation theory. The relevant partial differential equations are integrated in the artifical time dependent process, with the iterations as time steps (JAMESON [22]). Extensive work based on relaxation schemes has been completed in France. This is surveyed in the general paper by CHATTOT [3].

By contrast, the quasi-analytic methods make it possible to dispense with finite differences at least in one coordinate direction. The three methods of this type are the Method of Integral Relations, Telenin's Method, and the Method of Lines. These techniques were chiefly developed in the Soviet Union. The theory on which these methods are based as well as abundant applications and further references, is found in the monograph by HOLT [19]. The Method of Integral Relations was originally formulated by DORODNITSYN [7], and has subsequently been applied to a variety of fluid dynamics problems. An excellent account of the method for inviscid flow problems is given by Belotserkovskii and Chushkin in HOLT [18]. Telenin's Method was developed by GILIŃSKII, TELENIN and TINYAKOV [13] and others in order to solve the inviscid equations in the transonic region of supersonic flows past blunt bodies. HOLT and NDEFO [21], FLETCHER [11], and HOLT and CHAN [19] have used Telenin's Method to determine all or part of the solutions of steady supersonic flows past cones with successively more difficult constraints on the flow, namely moderate angles of attack, high angles of attack, and viscosity effects. The method consists of approximating the dependent variables in polynomials of one of

the independent variables as in the Method of Integral Relations. As a consequence, for a two-dimensional problem, a system of ordinary differential equations is again obtained. CHATTOT [3], has applied Telenin's Method to the symmetric flow past a double wedge in a high subsonic free stream. In general, Telenin's Method and the Method of Integral Relations are appropriate for numerical solutions using techniques of the following two general types:

1) finite difference methods, and
2) quasi-analytic methods.

In the first category, both Time Dependent Method and Relaxation Methods are used. The Time Dependent Method attempts to solve the direct equations by reformulating the boundary value problem as an initial-boundary value problem, following the introduction of time-dependent terms. As a consequence, the governing partial differential equations become purely hyperbolic. Several finite difference schemes have been successfully used to integrate the equations forward in time. Convergence of the transient solution to the steady state solution of the original problem is achieved provided the boundary conditions become or remain time-independent at large times. RICHTMYER and MORTON [35] give a general discussion of the method. Application of the method to transonic flow has been made by MAGNUS and YOSHIHARA [26] and GROSSMAN and MORETTI [15]. The Relaxation Method was first applied to external transonic flow with embedded shock waves by EMMONS [8, 9]. The transonic small perturbation equations have been integrated by MURMAN and COLE [29] and MURMAN and KRUPP [30] by reformulating the Relaxation Method used initially by Emmons. In their papers the mixed finite difference scheme is used to take into account the local behavior and domain of dependence of the differential equations. The full inviscid equations have been solved using technique by STEGER and LOMAX [36]. Attempts are currently being made to extend the calculations to three-dimensional inviscid flow as well as to two-dimensional viscous flow. It is worthwhile to note here that, for a slowly converging Relaxation Method, a good estimate of the over-relaxation factor can be made by regarding the relaxation scheme as a discrete approximation to problems governed by partial differential equations of elliptic, mixed elliptic-hyperbolic, and parabolic types. Finally, the Method of Lines differs from Telenin's Method only in one significant respect: the former adopts local interpolation over 3 to 5 points, while in the latter interpolation extends over a whole range in a coordinate direction. GROSS [14] has investigated symmetric, shock free, supercritical flows past ellipses using Telenin's Method and, alternatively, the Method of Lines. He solved the resultant ordinary differential equations as an initial value or Cauchy-type problem. To have sufficient Cauchy data, missing conditions at a boundary are guessed iteratively until the conditions at the outer boundary are satisfied as a result of the integration. Convergence of the iteration is technically speeded up by POWELL's [33, 34] method.

1.3. Outline of the present work

This paper is a reformulation and extension of an earlier transonic calculation by CHATTOT [3]. The steady supercritical transonic flow of an inviscid gas past a two-dimensional symmetric double wedge at a small angle of attack is analyzed in the hodograph

plane, assuming the flow to be isentropic and irrotational. Then the flow is transformed back to the physical plane. Along the wedge surface the stagnation points are assumed to be attached at the sharp leading and trailing vertices, and the sonic speed is, *a priori*, attained at the shoulders of the double wedge. The above assumption concerning the stagnation points is necessary for an inviscid fluid model since otherwise the flow would be indeterminate in the separated flow region following a sharp turn in the flow direction at the leading vertex. The mathematical boundaries and the corresponding flow domain are constructed in the hodograph plane and are seen to be contained within two sheets of a Riemann surface, which are subsequently separated by a cut introduced along a branch line. Two boundary value problems, one for the stream function and the other for the velocity potential, are formulated in each of the two Riemann sheets. The first problem consists of Chaplygin's equation and boundary conditions specified along the dividing streamlines, wedge surface, and in the far field. Along the dividing streamlines and wedge surfaces the condition of constant stream function applies and for the far field condition GERMAIN's [12] term is used. On the other hand, the second problem consists of another partial differential equation of mixed type, which is similar to Chaplygin's equation, with inhomogeneous Dirichlet type conditions on the boundary. The two boundary value problems are solved numerically in the mixed elliptic-hyperbolic hodograph domain using Telenin's method and a double sweep method. A closed body requirement, which is needed to recover the original physical configuration of the double wedge when the flow is mapped back to the physical plane, enables us to determine the shock foot positions. Starting from these points a pair of cuts is constructed in the two Riemann sheets such that, on the physical discontinuity curves corresponding to the hodograph cuts, the stream function and the velocity potential are continuous and the slope of the curves is single-valued. One of these two continuity conditions could be replaced by the Rankine–Hugoniot shock relations, since for a free stream of near-sonic speed the shock at the shoulder of the thin wedge will be so weak that the entropy changes across the discontinuity curve will be negligibly small. Such cuts eliminate those parts of the hodograph domain which contribute to the physically anomalous three-sheeted flows. Across the discontinuity curves in the physical plane there occur jumps of flow variables such as velocity, pressure and density, but not the integrated variables, stream function and velocity potential. This whole procedure is called shock fitting. Each of the fitted shocks has its foot at the shoulder of the double wedge and its tip is located at the double point where two physical limit lines form a cusp. Finally, by properly relating the solutions obtained in the two Riemann sheets aerodynamic characteristics are obtained.

2. Qualitative description of the flow

2.1. The physical flow field

VINCENTI and WAGONER [39] have investigated the aerodynamic characteristics, at a small angle of attack, of a thin double-wedge profile over the range of supersonic flight speeds for which a detached bow wave exists ahead of the wedge. In their work the effects

of the angle of attack are regarded as a small perturbation of the flow previously calculated at the zero angle of attack. The authors used relaxation procedures in the hodograph plane to solve Tricomi's equation for the mixed flow region and the method of characteristics for the purely supersonic region behind the shocks attached at the wedge shoulders. Transonic flow past a lifting double wedge in a sonic free stream is described in FERRARI and TRICOMI [10].

For a free-stream speed slightly less than sonic, the physical flow field is similar in its general features, but has the distinctive aspect that each of the embedded supersonic pockets in the subsonic flow is completely bounded by the sonic line and terminating shock wave, both of which originated from the wedge shoulder (see Fig. 1). Further,

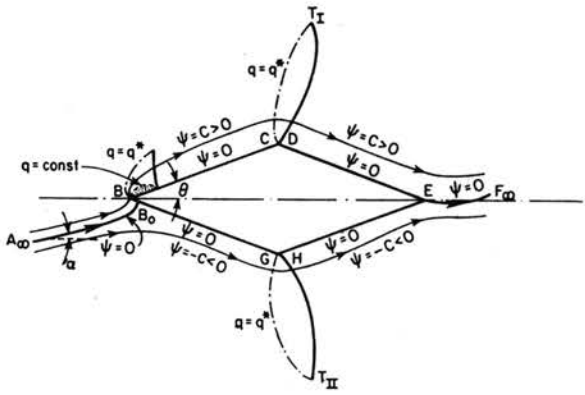

FIG. 1. Physical flow past a double wedge.

there are no recompression shocks occurring at the tail of the double wedge. The leading stagnation point (B_0), which stays at the leading vertex (B) of the double wedge at the zero angle of attack, moves downstream with an increase in the angle of attack. It moves onto the lower forward wedge surface and its distance from the leading vertex is unknown *a priori*. The dividing streamline $\psi = 0$ is curved near the leading stagnation point B_0 before it impinges normally on the lower forward surface and then follows the contour of the double wedge. The lower half of the flow field, that is, the flow below the dividing and zero streamline $\psi = 0$, is qualitatively similar to symmetric flow. Starting from the forward stagnation point, the streamline $\psi = 0$ moves a certain distance upstream along the lower forward surface before it experiences a sudden sharp turn around the nose B. This sharp turn is achieved by means of a Prandtl–Meyer expansion up to supersonic speed, generating the first supersonic region attached at the very front tip on the upper forward surface of the double wedge. However, for a thin double wedge the turning angle exceeds 130°, which is the limit for expansion to a vacuum. As a consequence, the streamline $\psi = 0$ is detached at the vertex B to allow a separated flow at the front tip on the upper forward surface. Nevertheless, experimental evidence shows that for a small angle of attack and for a free stream of near-sonic speed the flow is reattached to the upper forward surface, confining the separated bubble to a small closed region. The streamline $\psi = 0$ therefore follows the free surface of the bubble up to the point of reattachment

before it follows the rest of the upper forward wedge surface. The reattachment in the physical flow is actually brought about by the action of an oblique shock located at the point of reattachment. There are additional and more significant supersonic regions near the shoulders of the double wedge as a result of acceleration of the flow along the forward faces and local Prandtl–Meyer expansions at the shoulders, i.e. the convex corners C and G. The regions are bounded by sonic lines and terminating shocks. For a small angle of attack the rear stagnation point is, unlike the leading one, attached at the tail E of the double wedge leading to a dividing, slightly curved, streamline downstream.

The difficulty in the analysis of the asymmetric problem comes from the separated bubble which virtually alters the effective airfoil profile. The bubble pressure is indeterminate unless viscosity is considered and the boundary of the bubble is not well determined experimentally. A practical assumption made at this stage is that for a sufficiently small angle of attack the separated bubble plus its peripheral embedded supersonic flow region occupy only a very small part of the entire flow field near the vertex B of the double wedge. In consequence, the bubble effect may be considered to be of only secondary importance and can be neglected in the first approximation. Various authors, such as GUDERLY and YOSHIHARA [16], VINCENTI and WAGONER [39], and FERRARI and TRICOMI [10], neglected the bubble effect and this procedure is also followed in the present paper. As a consequence, the leading stagnation point is brought back to the nose of the double wedge and the curvature of the dividing streamline impinging on it is thereby reduced.

2.2. The hodograph flow field

The analysis of transonic flow past two-dimensional airfoils of wedge type has the advantage that most of the hodograph flow domain is known *a priori*. For a double wedge at the angle of attack the physical flow field maps onto two sheets of a Riemann surface in the hodograph plane, one sheet for the upper half of the physical flow field and the other for the lower half. The branch line common to the two Riemann sheets is, to a good approximation, the image of the forward and rear dividing streamlines, the curvature of which is assumed small near the two stagnation points. The flow at infinity in the physical plane is represented in the hodograph plane by a branch point. To make the hodograph

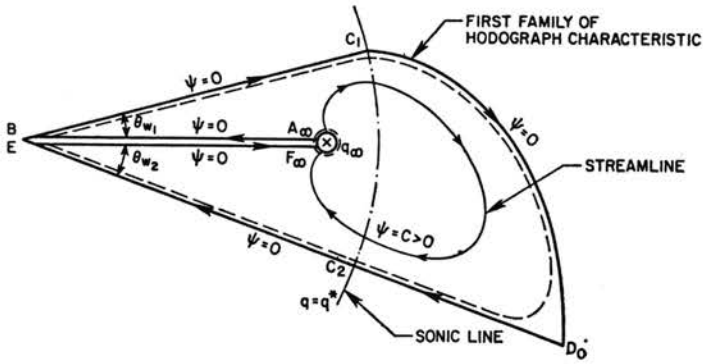

FIG. 2. First Riemann surface of the hodograph plane.

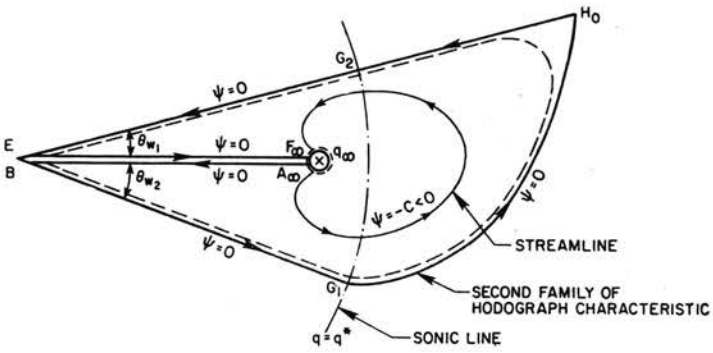

FIG. 3. Second Riemann surface of the hodograph plane.

flow domain analytic, a small circle is introduced at the singular branch point and a cut is made along the branch line. In Figs. 2 and 3 the two Riemann sheets are shown separately. Asymmetry of the two becomes evident when the wedge is set at the angle of attack. Nevertheless, in the first part of this paper, it suffices to describe the procedures in only one of the two Riemann sheets since the behavior in the two sheets is similar.

Following the streamline $\psi = 0$ in the first Riemann sheet of Fig. 2, the flow along the upper forward surface BC_1 is inclined at a constant angle θ_{w_1} $(\theta_w - \alpha > 0)$, where θ_w is the half wedge angle. At the apex C_1 there occurs a local Prandtl–Meyer expansion represented by the epicycloid C_1D_0. The flow is turned by the expansion through the wedge angle to follow the upper rear surface D_0E, which is inclined at another constant angle $-\theta_{w_2}$ $(-\theta_w - \alpha < 0)$. The points B, C_1, D_0 and E are all singular points at which first and possibly higher derivatives do not exist. At the stagnation points B and E, mathematical difficulties can be avoided since, in their neighborhood, the solution is known from the incompressible potential flow theory. The singularities at C_1 and D_0 are removed by replacing the hodograph boundary BC_1D_0E as an approximation by a highly-curved analytic contour closely following the original boundary: see the dotted lines in Figs. 2 and 3.

3. Mathematical formulation

3.1. Hodograph transformation

The steady two-dimensional, asymmetric, inviscid transonic flow under consideration is generated by a thin symmetrical double wedge at a small angle of attack in a high subsonic free stream. The flow is assumed to be irrotational and isentropic. From the irrotationality condition and the continuity equation, we can write

$$\begin{bmatrix} \phi_x & \phi_y \\ \psi_x & \psi_y \end{bmatrix} = \begin{bmatrix} u & v \\ -\varrho v & \varrho u \end{bmatrix}. \tag{3.1}$$

In the above ϕ, ψ, u, v, ϱ, x and y are all dimensionless variables scaled respectively as follows: u and v are velocity components divided by the maximum velocity $\tilde{q}_{\max}$; ϱ is the

density divided by the stagnation density $\tilde{\varrho}_0$; x and y are scaled with the chord $\tilde{c}$ of the double wedge; ϕ and ψ are the velocity potential and stream function, respectively, both made dimensionless in terms of the composite quantity $\tilde{q}_{\max} \cdot \tilde{c}$. Here and in what follows, any constant or variable with a tilde above it will imply that the quantity is dimensional. Inversion of Eq. (3.1) gives, with $q^2 = u^2+v^2$,

$$\begin{bmatrix} x_\phi & x_\psi \\ y_\phi & y_\psi \end{bmatrix} = \frac{1}{\varrho q^2} \begin{bmatrix} \varrho q\cos\theta & -q\sin\theta \\ \varrho q\sin\theta & q\cos\theta \end{bmatrix}. \tag{3.2}$$

Multiplying both sides of Eq. (3.2) by the matrix $\begin{bmatrix} \phi_q & \phi_\theta \\ \psi_q & \psi_\theta \end{bmatrix}$, we obtain

$$\begin{bmatrix} x_q & x_\theta \\ y_q & y_\theta \end{bmatrix} = \begin{bmatrix} \cos\theta/q & -\sin\theta/\varrho q \\ \sin\theta/q & \cos\theta/\varrho q \end{bmatrix} \begin{bmatrix} \phi_q & \phi_\theta \\ \psi_q & \psi_\theta \end{bmatrix}. \tag{3.3}$$

When the complex coordinate $z = x+iy$ is introduced, the above becomes

$$\begin{aligned} \partial z/\partial q &= \frac{1}{q} e^{i\theta}\left(\phi_q + i\frac{1}{\varrho}\psi_q\right), \\ \partial z/\partial\theta &= \frac{1}{q} e^{i\theta}\left(\phi_\theta + i\frac{1}{\varrho}\psi_\theta\right). \end{aligned} \tag{3.4}$$

Eliminating z from the above two equations by cross-differentiation, and equating real and imaginary parts, we have

$$\begin{aligned} \phi_q &= q\frac{d}{dq}\left(\frac{1}{\varrho q}\right)\psi_\theta, \\ \phi_\theta &= \frac{q}{\varrho}\psi_q, \end{aligned} \tag{3.5}$$

where the density is given by (γ is the ratio of specific heats)

$$\varrho = (1-q^2)^{1/(\gamma-1)}. \tag{3.6}$$

Equation (3.6) is obtained from Bernoulli's equation

$$\tilde{q}d\tilde{q} + \frac{d\tilde{p}}{\tilde{\varrho}} = 0$$

and the reversible adiabatic energy equation

$$\frac{2}{\gamma-1}\tilde{a}^2 + \tilde{q}^2 = \tilde{q}_{\max}^2, \quad \tilde{a}^2 \equiv \frac{d\tilde{p}}{d\tilde{\varrho}}.$$

The mapping relation is then

$$dz = z_q dq + z_\theta d\theta, \tag{3.7}$$

where the derivatives z_q and z_θ are given by Eqs. (3.4). These equations can have more explicit expressions in terms of the stream function ψ in the polar coordinates (q, θ) when ϕ and ϱ are eliminated by means of Eqs. (3.5) and (3.6). They are

$$x_q = -\frac{1}{\varrho q}\left[\sin\theta\psi_q + \frac{\cos\theta}{q}\,\frac{1-\dfrac{\gamma+1}{\gamma-1}q^2}{1-q^2}\,\psi_\theta\right], \tag{3.8}$$

(3.8) [cont.]

$$x_\theta = \frac{1}{\varrho q}[q\cos\theta\psi_q - \sin\theta\psi_\theta],$$

$$y_q = \frac{1}{\varrho q}\left[\cos\theta\psi_q - \frac{\sin\theta}{q}\frac{1-\frac{\gamma+1}{\gamma-1}q^2}{1-q^2}\psi_\theta\right],$$

$$y_\theta = \frac{1}{\varrho q}[q\sin\theta\psi_q + \cos\theta\psi_\theta].$$

3.2. Governing equations and boundary conditions

Equations (3.5) can be combined into a single expression by cross-differentiation. When Eq. (3.6) is used to eliminate the density dependence from the resultant equation, we obtain

$$\psi_{qq} + \frac{1-\frac{\gamma+1}{\gamma-1}q^2}{q^2(1-q^2)}\psi_{\theta\theta} + \frac{1+\frac{3-\gamma}{\gamma-1}q^2}{q(1-q^2)}\psi_q = 0. \tag{3.9}$$

This is the governing partial differential equation for the stream function in the hodograph polar coordinates (q, θ) and is called Chaplygin's equation. It is noted that this equation is now linear but still remains of mixed type regardless of the coordinate transformation. This is because the equation becomes elliptic in the subsonic region of the flow domain where $q < [(\gamma-1)/(\gamma+1)]^{1/2}$, and hyperbolic in the supersonic subdomain where $[(\gamma-1)/(\gamma+1)^{1/2} < q < 1$. It is also noted that, since the equation itself is homogeneous, inhomogeneous boundary conditions are expected to be specified in order to generate a nontrivial solution of the problem.

The boundary condition on the wedge surface and along the dividing streamlines is straightforward physically. On these boundaries the stream function remains constant and, for convenience of formulation, it will be taken equal to zero hereafter. In formal notation, along the hodograph boundary $A_\infty BC_1 D_0 EF_\infty$ in the first Riemann sheet and $A_\infty BG_1 H_0 EF_\infty$ in the second Riemann sheet, it is

$$\psi(q, \theta) = 0. \tag{3.10}$$

The second boundary is given in the far field of the physical flow or in the neighborhood of the singular branch point in the hodograph plane. Physically the condition states that, at distances sufficiently far from the body, the streamlines align more and more closely to the free stream since the disturbances become infinitesimally small there. GROSS [14] used a first-order doublet solution of the Prandtl–Glauert equation as a far-field condition applicable at some finite distance from the body in the subsonic flow region. The accuracy increases asymptotically as the distance from the body is increased. For the present problem of transonic flow, we use an asymptotic far field condition in the hodograph plane due to GERMAIN [12]. This is valid in the neighborhood of the branch point, which is located in the subsonic region. Mathematically we begin with the following two definitions:

$$\sigma = -\int_1^q \frac{\varrho(q)}{q} dq, \tag{3.11}$$

$$L(\sigma) = \frac{1}{\varrho^3} \frac{d}{dq}(\varrho q). \tag{3.12}$$

Equations (3.5) then readily reduce to the simpler form

$$\begin{aligned} \phi_\theta &= \psi_\sigma, \\ \phi_\sigma &= L(\sigma)\psi_\theta, \end{aligned} \tag{3.13}$$

from which the hodograph partial differential equation in Frankl's canonical form follows immediately:

$$\psi_{\sigma\sigma} + L(\sigma)\psi_{\theta\theta} = 0. \tag{3.14}$$

Define a new independent variable s such that

$$s(\sigma) = \int_0^\sigma [L(\sigma)]^{1/2} d\sigma. \tag{3.15}$$

Then, Eq. (3.14) becomes in the (s, θ) coordinates

$$\psi_{\theta\theta} + \psi_{ss} - \Lambda(s)\psi_s = 0, \tag{3.16}$$

where

$$\Lambda(s) = -\frac{1}{2}[L(\sigma)]^{-3/2} \frac{d}{d\sigma} L(\sigma). \tag{3.17}$$

Further, by defining a new stream function

$$\psi^* = [L(\sigma)]^{1/4}\psi, \tag{3.18}$$

we obtain a hodograph equation of the canonical elliptic type, which holds in the subsonic region of the flow domain,

$$\psi^*_{\theta\theta} + \psi^*_{ss} - N(s)\psi^* = 0, \tag{3.19}$$

where

$$N(s) = \frac{1}{4}[L(\sigma)]^{-3}\left[L(\sigma)\frac{d^2}{d\sigma^2}L(\sigma) - \frac{5}{4}\left(\frac{d}{d\sigma}L(\sigma)\right)^2\right]. \tag{3.20}$$

From Eq. (3.19) we can obtain an asymptotic expression for the stream function $\psi^*(s, \theta)$ in the neighborhood of the point at infinity A_∞ (or F_∞), with the leading term

$$\psi^*(s, \theta) = Ar^{-1/2}\sin\left(\frac{\tau}{2} + \alpha'\right), \tag{3.21}$$

where

$$\begin{aligned} r^2 &= \theta^2 + (s - s_\infty)^2, \\ \sin\tau &= \frac{\theta}{r}. \end{aligned} \tag{3.22}$$

In the above, A is an amplification constant and α' is a constant accounting for the angle of attack effect. Then the second boundary condition is given by Eq. (3.21) which applies asymptotically in the neighborhood of the branch point A_∞.

The partial differential equation governing the velocity potential $\phi(q,\theta)$, which is obtained when ψ and ϱ are eliminated from Eqs. (3.5) and (3.6), is given by

$$\phi_{qq}+\frac{1-\frac{\gamma+1}{\gamma-1}q^2}{q^2(1-q^2)}\phi_{\theta\theta}+\frac{\left(1-\frac{3\gamma-1}{\gamma-1}q^2\right)\left(1-\frac{\gamma+1}{\gamma-1}q^2\right)+2\frac{\gamma+1}{\gamma-1}q^2(1-q^2)}{q(1-q^2)\left(1-\frac{\gamma+1}{\gamma-1}q^2\right)^2}\phi_q=0, \tag{3.23}$$

which differs from Chaplygin's equation only in the coefficient of the first order derivative. The boundary condition along the dividing streamlines and on the double wedge surface is

$$\mathrm{grad}\phi\cdot\mathbf{n}=0, \tag{3.24}$$

where $\mathbf{n}$ is a unit normal vector at a point on the boundary. Alternatively, if the stream function is solved first, a more convenient mathematical condition can be adopted on the above boundaries, namely,

$$d\phi=\phi_x dx+\phi_y dy \tag{3.25}$$

or

$$d\phi=q(\cos\theta x_q+\sin\theta y_q)dq+q(\cos\theta x_\theta+\sin\theta y_\theta)d\theta. \tag{3.26}$$

When the mapping relations Eqs. $(3.8)_1$–$(3.8)_4$ are used, the increment of the velocity potential $d\phi$ is completely described in terms of the stream function in the hodograph polar coordinate system (q,θ). In the far field of the flow domain another asymptotic expression, such as Germain's term, would be appropriate for the velocity potential. In the present work, however, Eq. (3.26) is used again, which yields Dirichlet type boundary conditions when integrated.

3.3. Limit lines and shock fitting equations

It will first be shown, for later reference, that the streamlines are orthogonal to the equipotential lines in the physical plane of a two-dimensional steady compressible potential flow. Along an equipotential line

$$d\phi=\phi_x dx+\phi_y dy=0, \tag{3.27}$$

$$\left(\frac{dy}{dx}\right)_\phi=-\frac{\phi_x}{\phi_y}=-\frac{u}{v}, \tag{3.28}$$

whereas on a streamline

$$d\psi=\psi_x dx+\psi_y dy=0, \tag{3.29}$$

$$\left(\frac{dy}{dx}\right)_\psi=-\frac{\psi_x}{\psi_y}=\frac{\varrho v}{\varrho u}=\frac{v}{u}. \tag{3.30}$$

Therefore

$$\left(\frac{dy}{dx}\right)_\psi\left(\frac{dy}{dx}\right)_\phi=-1. \tag{3.31}$$

Thus the two families are orthogonal. CRAGGS [5] shows that any point which is singular of order one lies on a singular curve. Here a limit line is defined by a singular curve at each point of which the Jacobian of the transformation from the hodograph to physical plane vanishes. Not both of its derivatives vanish, however.

Applying a series of theorems due to Craggs, LIGHTHILL [25] demonstrated several properties. First, the limit line in the physical plane (the physical curve corresponding to the hodograph limit line) is, except near a cusp point if the limit line is cusped,

1) an envelope of one family of characteristics,

2) a cusp-locus of streamlines, equipotential lines, and the other family of characteristics. Further, all these curves lie on the same side of the limit line.

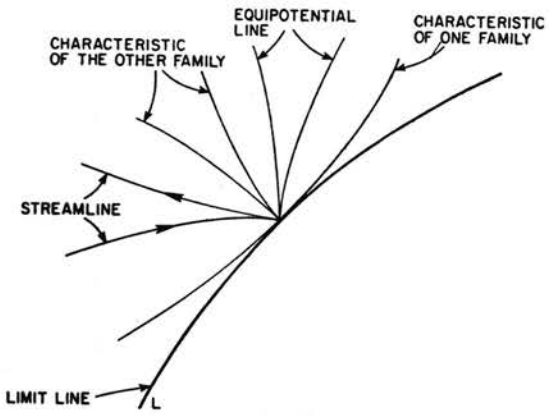

FIG. 4. Ordinary point of a limit line in the physical plane.

In Fig. 4 the above properties are illustrated, following Lighthill. Lighthill also showed that, at a cusp point of a cusped limit line,

1) the families of curves touching the limit line at ordinary points do so also at the cusp point, and

2) those curves having cusps at ordinary points of the limit line pass directly through the cusp point of the limit line.

These results are illustrated in Fig. 5. Furthermore, on a limit line in the hodograph plane, both the streamlines and the equipotential lines touch the characteristics of one family at ordinary points of the limit line. At a point corresponding to the cusp the streamline and the equipotential line osculate a characteristic. As a partial proof of this, we show that the streamline and the equipotential line are tangent at a point of the hodograph limit line. At a hodograph point (q, θ), the streamline has the expression

$$d\psi = \psi_q dq + \psi_\theta d\theta = 0, \tag{3.32}$$

$$\left(\frac{d\theta}{dq}\right)_\psi = -\frac{\psi_q}{\psi_\theta}, \tag{3.33}$$

whereas the equipotential line has

$$d\phi = \phi_q dq + \phi_\theta d\theta = 0, \tag{3.34}$$

(3.35) $$\left(\frac{d\theta}{dq}\right)_{\phi} = -\frac{\phi_q}{\phi_\theta}.$$

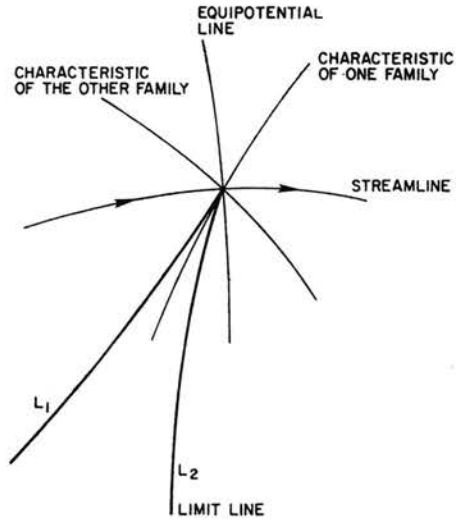

FIG. 5. Cusp point of a limit line in the physical plane.

If the point (q, θ) is on a limit line, the Jacobian of the transformation to the physical plane vanishes there, so that

(3.36) $$\frac{\partial(x, y)}{\partial(q, \theta)} = \frac{\partial(x, y)}{\partial(\phi, \psi)} \frac{\partial(\phi, \psi)}{\partial(q, \theta)} = \frac{1}{\varrho q^2} \frac{\partial(\phi, \psi)}{\partial(q, \theta)} = 0.$$

From Eqs. (3.33) and (3.35), using the last equation, it follows that on a hodograph limit line

(3.37) $$\left(\frac{d\theta}{dq}\right)_{\psi} = \left(\frac{d\theta}{dq}\right)_{\phi}$$

The proof of the properties is found in Lighthill's paper.

Limit lines, which occur only in the supersonic region, are physically unacceptable since the flow near a limit line is many-sheeted in the physical plane. Experimental observation shows that for the flow past wedge-type airfoils a shock wave appears near the wedge shoulder, approximately at the location of the theoretical limit lines in the physical plane. The existence of such a shock wave in the real fluid flow is strongly supported by the fact that in the theory the flow acceleration and pressure gradient become infinite at the limit lines so that irrotational flow breaks down due to the large friction and heat conduction effects. As a result, a shock or shocks have to be fitted into the solution found mathematically from the hodograph transformation. Now, suppose that Chaplygin's equation, with the given boundary conditions, is solved in the first Riemann sheet of the hodograph domain given by Fig. 2, and that the streamlines can be constructed as shown in Fig. 6.

The branch point A_∞ (or F_∞) behaves as a source or sink of the hodograph streamlines since the point A_∞ is the image of points at infinity in the physical flow field. The hodograph streamlines converge towards the branch point as the absolute value of the stream function increases from zero. In the supersonic subdomain a hodograph streamline, with an absolute value of the stream function less than a critical positive number, say C_2

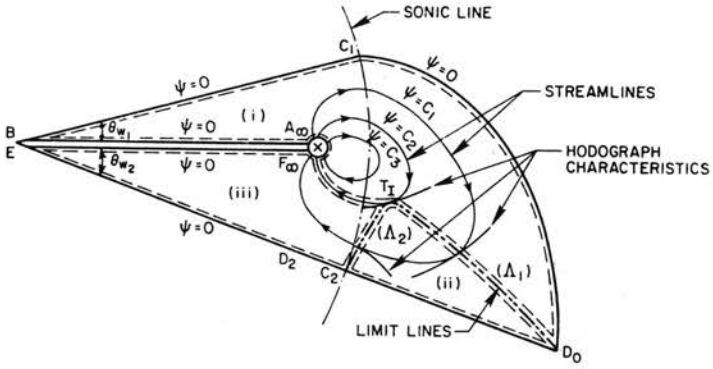

FIG. 6. Streamlines and limit lines in the first Riemann surface.

will have at least two points where the streamline is tangential to the hodograph characteristics. The loci of such points constitute a pair of limit lines Λ_1 and Λ_2 and at a point T_I it is seen that the streamline $\psi = C_2$ osculates a characteristic curve and the limit line $\Lambda_1+\Lambda_2$. Such a point is called a double point and, at a corresponding point in the physical plane, the two limit lines will form a cusp. The streamlines in the physical plane are cusped at each of the two limit lines in the upper half of the physical plane; this means that the flow is three-sheeted there. Also it should be noted that as a result, the rear faces of the double wedge protrude upstream, so that the original configuration of the double wedge is not obtained exactly. This awkward situation is due to the fact that the mathematical hodograph boundary and the corresponding flow domain contain a section which is physically redundant and, unfortunately, unknown *a priori*. In Figs. 6 and 7 the three-sheeted flow are distinguished by the numbers (i), (ii), and (iii). In Fig. 8 the equipotential lines are presented in the upper half of the physical plane and are also seen to be cusped at the limit lines. The equipotential lines cross the streamlines perpendicularly and therefore they intersect the wedge surface at right angles.

The difficulty brought about by the presence of the limit lines is overcome by introducing a discontinuity curve in the solution, as mentioned earlier. The construction of such a curve is subject to the following three fundamental conditions:

1) the hodograph discontinuity curve $D_1T_I+D_2T_I$ maps onto a single physical discontinuity curve DT_I (see Figs. 9 and 10),

2) the streamlines are continuous across the discontinuity curve DT_I in the physical plane, and

3) either the equipotential lines are continuous in the physical plane, or the Rankine–Hugoniot relations are satisfied.

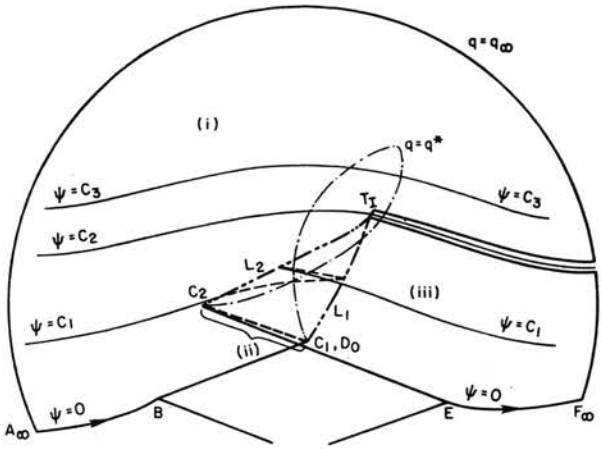

FIG. 7. Streamlines and limit lines in the upper half of the physical plane.

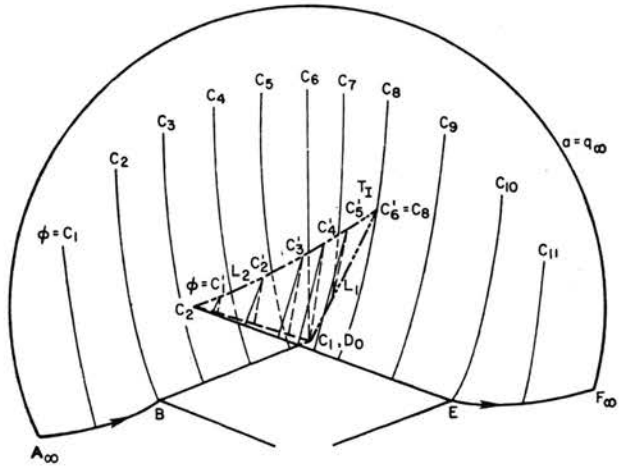

FIG. 8. Equipotentials and limit lines in the upper half of the physical plane.

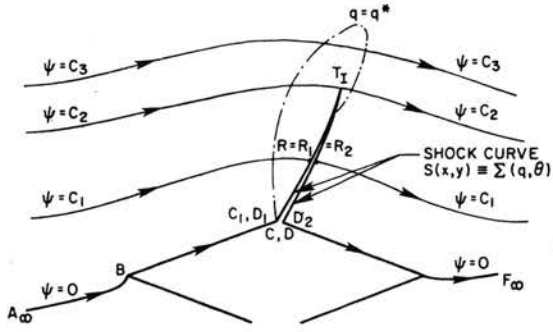

FIG. 9. Shock curve in the first Riemann surface.

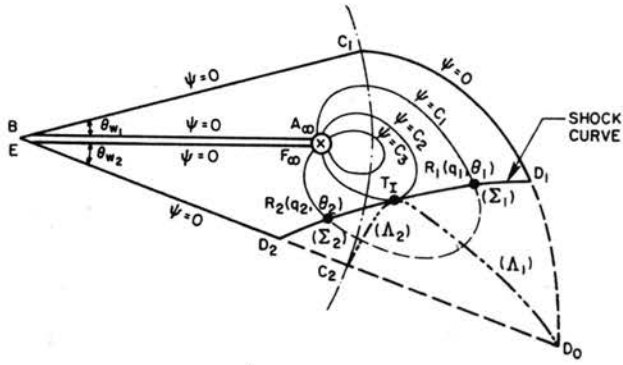

FIG. 10. Shock curve in the upper half of the physical plane.

The procedure determining such a discontinuity curve is called shock fitting, the curve being the shock wave. The shock foot is located at the wedge shoulder in the physical plane to satisfy the closed body requirement, which will be discussed in Sect. 5. In the hodograph plane the upstream point of the shock foot is, in turn, obtained from a shock relation. Starting from these two hodograph shock foot points the discontinuity curve can be obtained using the above three conditions. Now let (q_1, θ_1) and (q_2, θ_2) be the velocity vectors at the points immediately upstream and downstream of the shock, respectively [see the points $R_1(q_1, \theta_1)$ and $R_2(q_2, \theta_2)$ in Fig. 9 and the point $R(x, y) = R_1 = R_2$ in Fig. 10]. Let β be the magnitude of the angle of inclination of the physical shock curve at the point $R(x, y)$ and let $\beta' = \beta - \theta_1$ be the relative angle of inclination of the shock at the point R_1 measured from the incident flow direction in the physical plane. Also let $\delta = \theta_1 - \theta_2$ be the angle of flow deflection at the same shock point. Then the geometric relation between these variables is

$$\tan\beta' = -\frac{q_1 - q_2\cos\delta}{q_2\sin\delta}. \tag{3.38}$$

From this equation, the expression for β is obtained as

$$\tan\beta = \frac{q_1\cos\theta_1 - q_2\cos\theta_2}{q_2\sin\theta_2 - q_1\sin\theta_1}. \tag{3.39}$$

Then the condition (1) requires that the slope of the physical shock curve $S(x, y) = S(x(q, \theta), y(q, \theta)) = \Sigma(q, \theta)$ be single-valued at the physical point $R(x, y)$, which is the image of the two distinct hodograph points $R_1(q_1, \theta_1)$ and $R_2(q_2, \theta_2)$. Mathematically this condition can be written

$$\tan\beta = \left(\frac{dy}{dx}\right)_{S(x,y)} = \left(\frac{dy}{dx}\right)_1 = \left(\frac{dy}{dx}\right)_2, \tag{3.40}$$

where the transformations $dx(q, \theta)$ and $dy(q, \theta)$ are given, respectively, by the real and imaginary parts of Eq. (3.7). Equation (3.40) implies that the hodograph shock waves $\Sigma_1(q_1, \theta_1)$ and $\Sigma_2(q_2, \theta_2)$, i.e. the curves D_1T_I and D_2T_I in Fig. 9, map onto one and the same physical shock wave $S(x, y)$, or the curve DT_I in Fig. 10, provided one and the same physical point D can be assigned to the upstream and the downstream hodograph

shock foot D_1 and D_2. This last requirement is realized by fulfilling the closed body condition: the exact configuration of the double wedge is recovered by the shock foot which rests at the wedge shoulder. Now when dx and dy are replaced by their explicit expressions in the (q, θ) coordinates, we have

$$\frac{dy}{dx} = \frac{A(d\theta/dq)+B}{C(d\theta/dq)+D}, \tag{3.41}$$

where

$$A(q,\theta) = q\sin\theta\psi_q + \cos\theta\psi_\theta,$$

$$B(q,\theta) = \cos\theta\psi_q - \frac{\sin\theta}{q}\,\frac{1-\dfrac{\gamma+1}{\gamma-1}q^2}{1-q^2}\,\psi_\theta,$$

$$C(q,\theta) = q\cos\theta\psi_q - \sin\theta\psi_\theta,$$

$$D(q,\theta) = -\sin\theta\psi_q - \frac{\cos\theta}{q}\,\frac{1-\dfrac{\gamma+1}{\gamma-1}q^2}{1-q^2}\,\psi_\theta.$$

By introducing Eq. (3.41) into the relation $(dy/dx)_1 = (dy/dx)_2$ in Eq. (3.40), we have, with the notation $A_1 = A(q_1, \theta_1)$, $A_2 = A(q_2, \theta_2)$, etc.,

$$\left(\frac{d\theta}{dq}\right)_2 = \frac{(B_2C_1 - A_1D_2)(d\theta/dq)_1 + (B_2D_1 - B_1D_2)}{(A_1C_2 - A_2C_1)(d\theta/dq)_1 + (B_1C_2 - A_2D_1)}. \tag{3.42}$$

Also from the relation $\tan\beta = (dy/dx)_1$, we have

$$\left(\frac{d\theta}{dq}\right)_1 = -\frac{B_1 - D_1\tan\beta}{A_1 - C_1\tan\beta}, \tag{3.43}$$

where $\tan\beta$ has the expression given by Eq. (3.39). Equation (3.42) with Eq. (3.43) forms an ordinary differential equation for the hodograph shock wave Σ_2. The other complementary conditions are

$$\psi(q_1, \theta_1) = \psi(q_2, \theta_2), \tag{3.44}$$

and

$$\phi(q_1, \theta_1) = \phi(q_2, \theta_2). \tag{3.45}$$

An alternative condition to either of Eqs. (3.44) and (3.45) would be the velocity jump condition across a shock, in the form

$$H(q_1, \theta_1, q_2, \theta_2) = 0. \tag{3.46}$$

Such a condition can be obtained explicitly from a shock polar without difficulty. The function H has the dimensionless form

$$H = \frac{\gamma-1}{2\gamma}\,\frac{q_1^2+q_2^2}{q_1^2+q_2^2} - \cos(\theta_1-\theta_2)\,\frac{\gamma+1}{2\gamma}\,\frac{q_1^2+2\dfrac{\gamma-1}{\gamma+1}+q_2^2}{q_1q_2} + \frac{1}{\gamma} + \cos^2(\theta_1-\theta_2). \tag{3.47}$$

These conditions determine the hodograph shock wave $\Sigma_1+\Sigma_2$ uniquely. NOCILLA [32] showed that the hodograph shock curve touches the limit line at the double point. As a matter of fact, it turns out that at this very special point in the hodograph plane the

streamline, the equipotential line, a characteristic curve of one family, and the hodograph shock wave all osculate the limit line $\Lambda_1+\Lambda_2$. In the physical plane the limit line L_1+L_2 is an envelope of characteristic curves and, as mentioned earlier, forms a cusp at the double point. Also, in the physical plane, the streamline, the equipotential line, and the characteristic of one family pass directly through the double point, whereas the characteristic of the other family and the shock wave touch the limit line at the double point. The last argument means that the shock strength becomes infinitesimal at the double point, which coincides with the tip of a fitted shock. To conclude this section, we note that a similar fitting procedure applies to the second Riemann surface to obtain another oblique shock wave attached at the second shoulder of the double wedge in the lower half of the physical plane.

4. Numerical integration

4.1. Rectangular computational coordinates

A new system of hodograph polar coordinates (η, ω) is chosen such that its origin is located at the branch point A_∞ (Fig. 11). The transformation is

$$q = (\eta^2+q_\infty^2+2\eta q_\infty\cos\omega)^{1/2}, \quad 0 \leqslant q < 1, \tag{4.1}$$

$$\theta = \tan^{-1}\left(\frac{\eta\sin\omega}{q_\infty+\eta\cos\omega}\right), \quad -\theta_{w_2} \leqslant \theta \leqslant \theta_{w_1},$$

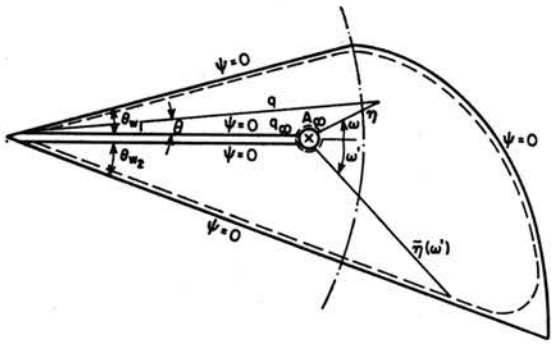

FIG. 11. Hodograph polar coordinates systems (q, θ) and (η, ω).

whereas the inverse transformation is

$$\eta = (q^2+q_\infty^2-2qq_\infty\cos\theta)^{1/2}, \quad 0 < \eta \leqslant \bar{\eta}(\omega), \tag{4.2}$$

$$\tan\omega = \frac{q\sin\theta}{q\cos\theta-q_\infty}, \quad -\pi \leqslant \omega \leqslant \pi,$$

where $\bar{\eta}(\omega)$ is the maximum radius at the given azimuthal angle ω. Now let Germain's term be applied at a finite distance from the double wedge in the physical plane, or in the hodograph plane in the neighborhood of the branch point, say at $\eta = \varepsilon(\omega)$, where

$0 < \varepsilon(\omega) \ll \bar{\eta}(\omega)$. Then a system of rectangular Cartesian coordinates (ξ, ω), shown in Fig. 12, is defined by

$$\xi = \frac{\eta - \varepsilon(\omega)}{\bar{\eta}(\omega) - \varepsilon(\omega)}, \quad 0 \leqslant \xi \leqslant 1,$$
$$\omega = \omega, \quad -\pi \leqslant \omega \leqslant \pi. \tag{4.3}$$

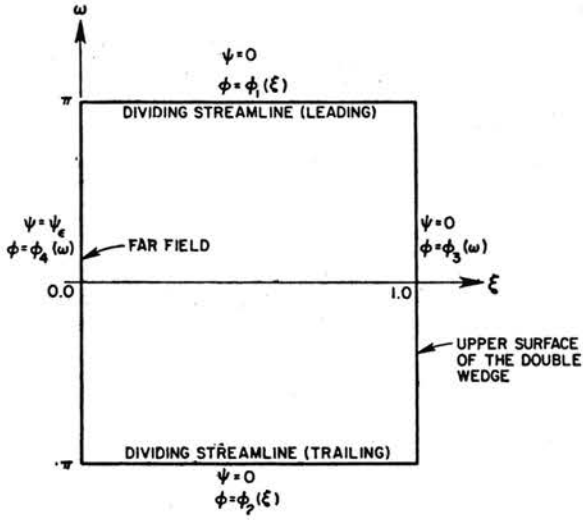

FIG. 12. Rectangular Cartesian coordinate system (ξ, ω).

Then Chaplygin's equation (3.9) transforms to

$$O(\xi, \omega)\psi_{\xi\xi} + P(\xi, \omega)\psi_{\xi\omega} + Q(\xi, \omega)\psi_{\omega\omega} + R(\xi, \omega)\psi_{\xi} + S(\xi, \omega)\psi_{\omega} = 0. \tag{4.4}$$

Before the expressions for the coefficients are given, functions of the dummy variables m and n are defined as follows:

$$f(m) = \left(\frac{\partial m}{\partial q}\right)^2 + M(q)\left(\frac{\partial m}{\partial \theta}\right)^2,$$
$$g(m, n) = \frac{\partial m}{\partial q}\frac{\partial n}{\partial q} + M(q)\frac{\partial m}{\partial \theta}\frac{\partial n}{\partial \theta}, \tag{4.5}$$
$$h(n) = \frac{\partial^2 n}{\partial q^2} + M(q)\frac{\partial^2 n}{\partial \theta^2} + N(q)\frac{\partial n}{\partial q},$$

where $M(q)$ and $N(q)$ are again

$$M(q) = \frac{1 - \dfrac{\gamma+1}{\gamma-1}q^2}{q^2(1-q^2)},$$
$$N(q) = \frac{1 + \dfrac{3-\gamma}{\gamma-1}q^2}{q(1-q^2)}. \tag{4.6}$$

Then the coefficients of Chaplygin's equation (4.4) have the form

$$O(\xi,\omega) = f(\eta)\left(\frac{\partial\xi}{\partial\eta}\right)^2 + 2g(\eta,\omega)\frac{\partial\xi}{\partial\omega}\frac{\partial\xi}{\partial\eta} + f(\omega)\left(\frac{\partial\xi}{\partial\omega}\right)^2,$$

$$P(\xi,\omega) = 2\left[g(\eta,\omega)\frac{\partial\xi}{\partial\eta} + f(\omega)\frac{\partial\xi}{\partial\omega}\right],$$

(4.7)
$$Q(\xi,\omega) = f(\omega),$$

$$R(\xi,\omega) = 2g(\eta,\omega)\frac{\partial^2\xi}{\partial\eta\partial\omega} + f(\omega)\frac{\partial^2\xi}{\partial\omega^2} + h(\eta)\frac{\partial\xi}{\partial\omega} + h(\omega)\frac{\partial\xi}{\partial\omega},$$

$$S(\xi,\omega) = h(\omega).$$

Next, Germain's condition (3.21) needs to be transformed to the new coordinate system. The integral for σ in the definition (3.11) has, in the case of a perfect gas ($\gamma = 1.4$), the following exact expression:

$$\sigma(q) = -\left[\frac{1}{5}\cos^5 t + \frac{1}{3}\cos^3 t + \cos t + \ln\tan\left(\frac{1}{2}t\right)\right]$$

with

$$t \equiv \sin^{-1} q.$$

Also, the definition (3.12) has the explicit form

$$L(q) = \frac{1}{\varrho^2}\left(1 - \frac{2}{\gamma-1}\frac{q^2}{1-q^2}\right),$$

where it is recalled that

$$\varrho(q) = (1-q^2)^{\frac{1}{\gamma-1}}.$$

Then the integral in Eq. (3.15) turns out to be

$$(4.8)_1 \qquad s - s_\infty = -\int_{q_\infty}^{q} \frac{1}{q}\left(1 - \frac{2}{\gamma-1}\frac{q^2}{1-q^2}\right)^{1/2} dq.$$

This integral has no closed form solution but can have an asymptotic expression in the neighborhood of the branch point A_∞, where the flow speed is q_∞. It is

$$(4.8)_2 \qquad s - s_\infty = -\frac{q-q_\infty}{q_\infty}\left(1 - \frac{2}{\gamma-1}\frac{q_\infty^2}{1-q^2}\right)^{1/2} \cdot H(q-q_\infty)$$

in which the function H is given by

(4.9)
$$H(\bar{\varepsilon}) = 1 - a\bar{\varepsilon} - b\bar{\varepsilon}^2 - c\bar{\varepsilon}^3 - \ldots,$$

where

$$\bar{\varepsilon} = q - q_\infty \quad (\bar{\varepsilon} \ll 1),$$

$$a = \frac{1}{2q_\infty}\left(\frac{\mu}{1-q_\infty^2} + 1\right),$$

$$b = \frac{1}{3q_\infty^2}\left[\frac{\mu^2 + \mu(5q_\infty^2 - 1)}{2(1-q_\infty^2)^3} - 1\right],$$

$$c = \frac{1}{4q_\infty^3}\left[\frac{\mu^3+4q_\infty^2\mu^2+\mu(1-2q_\infty^2+9q_\infty^4-4q_\infty^6+4q_\infty^8)}{2(1-q_\infty^2)^3}+1\right]$$

with the definition

$$\mu = \frac{1}{\gamma-1}\frac{q_\infty^2}{1-\dfrac{\gamma+1}{\gamma-1}q_\infty^2}.$$

Germain's condition (3.20) now becomes, at a point q near the point at infinity q_∞,

$$\psi(q,\theta) = A[L(q)]^{-1/4}[r(q,\theta)]^{-1/2}\sin\left(\frac{1}{2}\tau(q,\theta)+\alpha'\right), \tag{4.10}$$

where

$$r^2(q,\theta) = \theta^2+\frac{(q-q_\infty)^2}{q_\infty^2}\left(1-\frac{2}{\gamma-1}\frac{q_\infty^2}{1-q_\infty^2}\right)H^2(q-q_\infty),$$
$$\sin\left(\tau(q,\theta)\right) = \frac{\theta}{r(q,\theta)}. \tag{4.11}$$

Here the functions $L(q)$ and $H(q-q_\infty)$ are given by Eqs. (4.7) and (4.9), respectively. As mentioned earlier, A is an amplification constant and the constant α' accounts for the effect of the angle of attack. However, it is possible to drop the constant α' from consideration by aligning the x-coordinate with the free stream direction in the physical plane. Such a physical coordinate x has been chosen in this paper and the constant α' will not be considered henceforth. The amplification constant A is assigned the value unity for the time being in this section, but later, in Sect. 5.1, correction factors will be found in the two Riemann sheets by fulfilling the closed body requirement. In Eq. (4.11) care needs to be taken not to define a multiple-valued inversion. The inversion is taken here such that

$$\text{if} \quad 0 \leqslant \frac{\tau}{2} \leqslant \pi: \quad \psi \geqslant 0 \quad \text{(in the first Riemann sheet)},$$

$$\text{if} \quad -\pi \leqslant \frac{\tau}{2} \leqslant 0: \quad \psi \leqslant 0 \quad \text{(in the second Riemann sheet)}.$$

When Eq. (4.10) is transformed to the computational coordinate system (ξ,ω), we obtain the final form of Germain's condition. Recalling that Germain's term was evaluated at $\eta = \varepsilon(\omega)$, or $\xi = 0$, we denote the final form formally by

$$\psi(\xi,\omega)|_{\xi=0} = \psi_e(\omega), \quad -\pi \leqslant \omega \leqslant \pi. \tag{4.12}$$

The other boundary condition is on the double wedge surface

$$\psi(\xi,\omega)|_{\xi=1} = 0, \quad -\pi \leqslant \omega \leqslant \pi, \tag{4.13}$$

and along the dividing streamlines

$$\psi(\xi,\omega)|_{\omega=\pm\pi} = 0, \quad 0 \leqslant \xi \leqslant 1. \tag{4.14}$$

The governing partial differential equation for the velocity potential, Eq. (3.23), transforms in a way similar to Chaplygin's equation. In the computational coordinate

system (ξ, ω), it takes the same form as Eq. (4.4) with different expressions for the coefficients $R(\xi, \omega)$ and $S(\xi, \omega)$. If the function $N(q)$ in Eq. $(4.6)_2$ is altered to

$$N(q) = \frac{\left(1-\frac{3\gamma-1}{\gamma-1}q^2\right)\left(1-\frac{\gamma+1}{\gamma-1}q^2\right)+2\frac{\gamma+1}{\gamma-1}q^2(1-q^2)}{q(1-q^2)\left(1-\frac{\gamma+1}{\gamma-1}q^2\right)^2}, \tag{4.15}$$

then the governing equation can be written essentially in the same form as before, i.e.

$$O(\xi, \omega)\phi_{\xi\xi}+P(\xi, \omega)\phi_{\xi\omega}+Q(\xi, \omega)\phi_{\omega\omega}+R(\xi, \omega)\phi_{\xi}+S(\xi, \omega)\phi_{\omega} = 0, \tag{4.16}$$

where the coefficients are given by Eq. $(4.7)_1$–$(4.7)_5$ again. The boundary condition given by Eq. (3.26) transforms to

$$\begin{aligned} d\phi = {} & q[(\cos\theta x_q-\sin\theta y_q)q_\eta\eta_\xi+(\cos\theta x_\theta+\sin\theta y_\theta)\theta_\eta\eta_\xi]d\xi \\ & +q[(\cos\theta x_q+\sin\theta y_q)(q_\eta\eta_\omega+q_\omega)+(\cos\theta x_\theta+\sin\theta y_\theta)(\theta_\eta\eta_\omega+\theta_\omega)]d\omega. \end{aligned} \tag{4.17}$$

For the rectangular domain shown in Fig. 12, we have either $d\xi = 0$ or $d\omega = 0$ on each of the four boundaries and therefore the expression for the increment $d\phi$ in Eq. (4.17) takes a much simpler form there. When it is integrated, we obtain inhomogeneous boundary conditions of the form

$$\begin{aligned} \phi(\xi, \omega = \pi) &= \phi_1(\xi), \\ \phi(\xi, \omega = -\pi) &= \phi_2(\xi), \\ \phi(\xi = 1, \omega) &= \phi_3(\omega), \\ \phi(\xi = 0, \omega) &= \phi_4(\omega). \end{aligned} \tag{4.18}$$

For convenience of formulation in the following section, where a numerical technique known as Telenin's method is applied, the boundary conditions at $\omega = \pm\pi$ will be made homogeneous by defining a new velocity potential $\Phi(\xi, \omega)$. Consider the following definition:

$$\phi(\xi, \omega) = \Phi(\xi, \omega)+\frac{\pi+\omega}{2\pi}\phi_1(\xi)+\frac{\pi-\omega}{2\pi}\phi_2(\xi). \tag{4.19}$$

Then the new function $\Phi(\xi, \omega)$ is subject to the conditions

$$\begin{aligned} \Phi(\xi, \omega = \pi) &= 0, \\ \Phi(\xi, \omega = -\pi) &= 0, \\ \Phi(\xi = 1, \omega) &= \phi_3(\omega)-\frac{\pi+\omega}{2\pi}\phi_1(1)-\frac{\pi-\omega}{2\pi}\phi_2(1), \\ \Phi(\xi = 0, \omega) &= \phi_4(\omega)-\frac{\pi+\omega}{2\pi}\phi_1(0)-\frac{\pi-\omega}{2\pi}\phi_2(0) \end{aligned} \tag{4.20}$$

and is governed by a new, inhomogeneous partial differential equation

$$O(\xi, \omega)\Phi_{\xi\xi}+P(\xi, \omega)\Phi_{\xi\omega}+Q(\xi, \omega)\Phi_{\omega\omega}+R(\xi, \omega)\Phi_{\xi}+S(\xi, \omega)\Phi_{\omega} = T(\xi, \omega), \tag{4.21}$$

where the force function $T(\xi, \omega)$ is given by

$$T(\xi,\omega) = -\left(\frac{\pi+\omega}{2\pi}\phi_1'' + \frac{\pi-\omega}{2\pi}\phi_2''\right)O(\xi,\omega) - \left(\frac{1}{2\pi}\phi_1' - \frac{1}{2\pi}\phi_2'\right)P(\xi,\omega)$$
$$-\left(\frac{\pi+\omega}{2\pi}\phi_1' + \frac{\pi-\omega}{2\pi}\phi_2'\right)R(\xi,\omega) - \left(\frac{1}{2\pi}\phi_1 - \frac{1}{2\pi}\phi_2\right)S(\xi,\omega). \tag{4.22}$$

4.2. Telenin's method

Telenin's method presents an alternative to finite difference methods, at least in one coordinate direction, and has been successfully applied to many fluid mechanics problems. In this method the unknowns are approximated by interpolation polynomials, Lagrange or trigonometric, in one of the independent variables. In the present problems for the stream function and the velocity potential, noting that the homogeneous boundary conditions at $\omega = \pm\pi$ in the ω-direction are periodic for all ξ, we can best approximate the dependent variables by trigonometric polynomials.

To present the method of solution in a unified manner for both the stream function and the velocity potential formulation, let $\chi(\xi,\omega)$ denote either $\psi(\xi,\omega)$ or $\phi(\xi,\omega)$. Then our task is to solve a linear mixed partial differential equation of the form

$$A(\xi,\omega)\chi_{\xi\xi} + B(\xi,\omega)\chi_{\xi\omega} + C(\xi,\omega)\chi_{\omega\omega} + D(\xi,\omega)\chi_\xi + E(\xi,\omega)\chi_\omega = F(\xi,\omega) \tag{4.23}$$

in the domain $0 \leqslant \xi \leqslant 1$, $-\pi \leqslant \omega \leqslant \pi$ with the boundary conditions

$$\begin{aligned} \chi(\xi, \omega = \pi) &= 0, \\ \chi(\xi, \omega = -\pi) &= 0, \\ \chi(\xi = 1, \omega) &= a(\omega), \\ \chi(\xi = 0, \omega) &= b(\omega). \end{aligned} \tag{4.24}$$

Now if we approximate the unknown variable $\chi(\xi,\omega)$ by a trigonometric polynomial of the form

$$\chi(\xi,\omega) = \sum_{j=1}^{N} G_j(\xi)\sin\left(j\frac{\pi-\omega}{2}\right), \tag{4.25}$$

then the boundary conditions at $\omega = \pm\pi$, Eqs. $(4.24)_1$ and $(4.24)_2$ are certainly satisfied. If we define, for equally-spaced discrete values of ω_k, $k = 1, 2, \ldots, N$,

$$\chi_k(\xi) = \chi(\xi,\omega_k), \tag{4.26}$$

$$H_{ij} = \sin\left(j\frac{\pi-\omega_i}{2}\right), \tag{4.27}$$

$$h_{ij} = H_{ij}^{-1}, \tag{4.28}$$

then the coefficients in Eq. (4.25) satisfy the condition

$$G_j(\xi) = \sum_{i=1}^{N} h_{ij}\chi_i(\xi) \tag{4.29}$$

and Eq. (4.25) becomes

$$\chi(\xi,\omega)=\sum_{i=1}^{N}\sum_{j=1}^{N}h_{ij}\chi_i(\xi)\sin\left(j\frac{\pi-\omega}{2}\right). \tag{4.30}$$

From Eqs. (4.26) and (4.30), the derivatives of $\chi(\xi,\omega)$ are, for fixed values of ω_k, $k=$ $=1,2,\ldots,N$,

$$\chi_\xi(\xi,\omega_k)=\chi_k'(\xi),$$

$$\chi_{\xi\xi}(\xi,\omega_k)=\chi_k''(\xi),$$

$$\chi_\omega(\xi,\omega_k)=-\sum_{i=1}^{N}\sum_{j=1}^{N}\frac{j}{2}h_{ij}\chi_i(\xi)\cos\left(j\frac{\pi-\omega_k}{2}\right),$$

$$\chi_{\xi\omega}(\xi,\omega_k)=-\sum_{i=1}^{N}\sum_{j=1}^{N}\frac{j}{2}h_{ij}\chi_i'(\xi)\cos\left(j\frac{\pi-\omega_k}{2}\right),$$

$$\chi_{\omega\omega}(\xi,\omega_k)=-\sum_{i=1}^{N}\sum_{j=1}^{N}\left(\frac{j}{2}\right)^2h_{ij}\chi_i(\xi)\sin\left(j\frac{\pi-\omega_k}{2}\right).$$

Upon substituting into Eq. (4.23), we obtain

$$\chi_k''(\xi)-\sum_{i=1}^{N}[\varkappa_{ki}(\xi)\chi_i'(\xi)+\lambda_{ki}(\xi)\chi_i(\xi)]=\mu_k(\xi), \tag{4.31}$$

where

$$\varkappa_{ki}(\xi)=\frac{B(\xi,\omega_k)}{A(\xi,\omega_k)}(\Sigma_1)_{ki}-\frac{D(\xi,\omega_k)}{A(\xi,\omega_k)}\delta_{ki},$$

$$\lambda_{ki}(\xi)=\frac{C(\xi,\omega_k)}{A(\xi,\omega_k)}(\Sigma_2)_{ki}+\frac{E(\xi,\omega_k)}{A(\xi,\omega_k)}(\Sigma_1)_{ki}, \tag{4.32}$$

$$\mu_k(\xi)=\frac{F(\xi,\omega_k)}{A(\xi,\omega_k)},$$

where

$$(\Sigma_1)_{ki}=\sum_{j=1}^{N}\frac{j}{2}h_{ij}\cos\left(j\frac{\pi-\omega_k}{2}\right),$$

$$(\Sigma_2)_{ki}=\sum_{j=1}^{N}\left(\frac{j}{2}\right)^2h_{ij}\sin\left(j\frac{\pi-\omega_k}{2}\right),$$

$$\delta_{ki}=\begin{cases}1, & \text{if} \quad k=i,\\ 0, & \text{if} \quad k\neq i.\end{cases}$$

In vector notation Eq. (4.31) can be written, for $0\leqslant\xi\leqslant 1$,

$$f''(\xi)-K(\xi)f'(\xi)-\Lambda(\xi)f(\xi)=g(\xi), \tag{4.33}$$

where $f(\xi)$ is a vector with definition

$$f(\xi) = (\chi_1, \chi_2, \ldots, \chi_N)^T$$

and $K(\xi)$ and $\Lambda(\xi)$ are matrices the elements of which are given by Eqs. $(4.32)_1$ and $(4.32)_2$, respectively, and finally, $g(\xi)$ is a vector

$$g(\xi) = (\mu_1, \mu_2, \ldots, \mu_N)^T.$$

The two remaining boundary conditions are, from Eqs. $(4.24)_3$ and $(4.24)_4$,

$$f(\xi)|_{\xi=1} = \big(a(\omega_1), a(\omega_2), \ldots, a(\omega_N)\big)^T, \tag{4.34}$$

$$f(\xi)|_{\xi=0} = \big(b(\omega_1), b(\omega_2), \ldots, b(\omega_N)\big)^T. \tag{4.35}$$

The system, N coupled second-order ordinary differential equations represented by Eq. (4.33) and the two split boundary conditions given by Eqs. (4.34) and (4.35), constitutes a two-point boundary value problem, the solution of which is considered in the following section.

4.3. Two-point boundary value problems

To solve two-point boundary value problems, KELLER [23] gives a detailed account of shooting techniques. These techniques solve the problems as a sequence of initial value or Cauchy problems and are necessarily iterative methods. For the present problem these methods may exhibit difficulty of instability because of the mixed nature of the domain considered for the solution. In this report, to solve a system of coupled ordinary differential equations with split boundary conditions, a method due to BABENKO, VOSKRESENSKII, LYUBIMOV and RUSANOV [1], and NEWMAN [31] is used. It is essentially a finite difference approximation of the derivatives, followed by a double sweep method.

First, the coordinate ξ is divided by M equal mesh steps in the interval $0 \leqslant \xi \leqslant 1$. The derivatives in Eq. (4.33) are approximated by the central difference schemes

$$f''(\xi) = \frac{f_{n+1} - 2f_n + f_{n-1}}{\Delta^2} + O(\Delta^2), \tag{4.36}$$

$$f'(\xi) = \frac{f_{n+1} - f_{n-1}}{2\Delta} + O(\Delta^2), \tag{4.37}$$

where f_n is written for $f(\xi_n)$ and Δ is a step size. Then, for the interior points $n = 1, 2, \ldots, M-1$, we obtain a system of coupled algebraic equations

$$\left(I + \frac{\Delta}{2}K_n\right) f_{n-1} - (2I + \Delta^2 \Lambda_n) f_n + \left(I - \frac{\Delta}{2}K_n\right) f_{n+1} = \Delta^2 g_n, \tag{4.38}$$

where I is an identity matrix of order N. The boundary conditions are

$$f_M = \big(a(\omega_1), a(\omega_2), \ldots, a(\omega_N)\big)^T, \tag{4.39}$$

$$f_0 = \big(b(\omega_1), b(\omega_2), \ldots, b(\omega_N)\big)^T. \tag{4.40}$$

The system consisting of Eqs. (4.38)–(4.40) is, when combined, another matrix equation of the form $D\hat{f} = d$. Here D is a tri-block diagonal matrix, d is a vector of dimension $N(M-1)$ whose first and last elements contain the information from the boundary con-

ditions, Eq. (4.40) and Eq. (4.39), respectively, and $\hat{f}$ is the vector $(f_1^T, f_2^T, \ldots, f_{M-1}^T)^T$. The underlying concept of the double sweep method is that Gaussian elimination of a large matrix of order $N(M-1)$ is unnecessary because of the tri-block diagonal property of the matrix of the present problem. Instead, we can choose inversion of a matrix of smaller order N at each of the $(M-1)$ interior mesh points by assuming a special algebraic relation between two adjacent mesh points, such as

$$f_n = T_n f_{n+1} + t_n, \tag{4.41}$$

or

$$f_{n-1} = T_{n-1} f_n + t_{n-1}, \tag{4.42}$$

where T_n and t_n are the coefficient matrix and vector at the mesh point n, both unknown and of order N. Substituting Eq. (4.42) into Eq. (4.38), we obtain

$$f_n = W_n^{-1}\left(I - \frac{\Delta}{2}K_n\right) f_{n+1} + W_n^{-1}\left[\left(I + \frac{\Delta}{2}K_n\right) t_{n-1} - \Delta^2 g_n\right], \tag{4.43}$$

where

$$W_n = (2I + \Delta^2 \Lambda_n) - \left(I + \frac{\Delta}{2}K_n\right) T_{n-1}. \tag{4.44}$$

Comparing Eq. (4.43) with Eq. (4.41), we find

$$\begin{aligned} T_n &= W_n^{-1}\left(I - \frac{\Delta}{2}K_n\right), \\ t_n &= W_n^{-1}\left[\left(I - \frac{\Delta}{2}K_n\right) t_{n-1} - \Delta^2 g_n\right]. \end{aligned} \tag{4.45}$$

Setting $n = 0$ from Eq. (4.41) and using the boundary condition Eq. (4.40), we get

$$f_0 = T_0 f_1 + t_0 = \left(b(\omega_1), b(\omega_2), \ldots, b(\omega_N)\right)^T, \tag{4.46}$$

which is satisfied, for a finite vector f_1, if we choose

$$\begin{aligned} T_0 &= \mathbf{0}, \\ t_0 &= \left(b(\omega_1), b(\omega_2), \ldots, b(\omega_N)\right)^T. \end{aligned} \tag{4.47}$$

These two are the initial values for the coefficients T_n and t_n in the recurrence formulae, Eqs. $(4.45)_1$ and $(4.45)_2$. From these equations, as n increases from 1 to $(M-1)$, the coefficients T_n and t_n are determined successively, and this procedure is called the forward sweep. At the second boundary $\xi = 1$, from Eq. (4.42) with n set equal to M,

$$f_{M-1} = T_{M-1} f_M + t_{M-1}. \tag{4.48}$$

When the boundary condition Eq. (4.39) is used, since the coefficients T_{M-1} and t_{M-1} are known, the vector f_{M-1} can be evaluated. Initiated from this local solution of the problem, the solutions at the adjoining points $n = M-2, M-3, \ldots, 2, 1$ can be successively determined from Eq. (4.42). This procedure of back-substitution is called the reverse sweep. The two sweeps, forward and reverse, constitute a cycle of double sweep. This double sweep method has been successfully applied to nonlinear equations by BABENKO *et al.* [1] in solving supersonic inviscid three-dimensional flow past smooth bodies. At

a plane of constant matching coordinate, the character of the body condition is transferred by the forward sweep along a ray up to the shock position, where the rest of the boundary conditions are given. Flow variables are calculated in the backward sweep of the ray. Using the old values of unknowns in the coefficients of nonlinear algebraic equations, the unknowns in the current cycle of double sweep can be determined. With the appropriate relaxation factor, the iterative process converges rapidly.

5. Other preliminary formulae and results

5.1. Closed body condition

It was noted in Sect. 3.3 that the mathematical hodograph boundary constructed in Fig. 6 does not allow the original double wedge configuration to be reproduced in the physical plane. Elongation of the rear faces of the double wedge upstream, as seen in Figs. 7 and 8 for the upper rear face only, is due to the fact that the hodograph domain is analytic and certain parts of the hodograph boundaries are physically superfluous despite their mathematical consistency. Here a pair of cuts is needed in the two Riemann sheets to eliminate the redundant parts of the hodograph boundary and domain so that the original figure of the double wedge as well as a one-sheeted flow is retained.

Suppose that the curve $D_1 T_I D_2$ in Fig. 9 is the hodograph shock in the first Riemann sheet of the hodograph domain obtained by solving the shock fitting equations, and that the curve DT_I in Fig. 10 is the corresponding physical shock wave. In the second Riemann sheet, let the hodograph shock be represented by $H_1 T_{II} H_2$ (not shown) and the corresponding shock wave by HT_{II}. The initial value $\theta_2(q_2)$ for the shock-fitting ordinary differential equation (3.42) can be taken from the coordinates of the downstream shock feet, D_2 and H_2, in the first and second Riemann sheets, respectively. Now consider the following closed body condition in the physical plane

$$\oint_{\text{Body}} dz = 0, \tag{5.1}$$

where $z = x+iy$. The surface of the double wedge has, in the hodograph domain where a pair of shocks $D_1 T_I D_2$ and $H_1 T_{II} H_2$ is fitted in the image $BC_1 D_1 \cap D_2 E \cap E H_2 \cap H_1 G_1 B$. The hodograph characteristic curves $C_1 D_1$ and $G_1 H_1$ of the hodograph boundary span zero distance in the physical plane since they are the images of isolated physical points, the shoulders of the double wedge. Then the real part of Eq. (5.1) can be put in the form

$$\int_{BC_1} dx + \int_{D_2 E} dx = \int_{BG_1} dx + \int_{H_2 E} dx = \cos\alpha. \tag{5.2}$$

Further, due to the symmetry of the double wedge in the chord direction, the following relations hold:

$$\begin{aligned} X_I &\equiv \int_{BC_1} dx = \frac{\cos\theta_{w_1}}{\cos\theta_{w_2}} \int_{D_2 E} dx, \\ X_{II} &\equiv \int_{BG_1} dx = \frac{\cos\theta_{w_2}}{\cos\theta_{w_1}} \int_{H_2 E} dx. \end{aligned} \tag{5.3}$$

In the hodograph plane along the wedge face images BC_1, D_2E, BG_1 and H_2E, flow inclinations are constant and therefore the derivatives of the stream function in those directions vanish. Then we have the condition $d\theta = 0$ and also the condition $\partial\psi/\partial q = 0$ on the above images. With θ_s used to denote the angle of wall inclination, which is either θ_{w_1} or $-\theta_{w_2}$, the increment dx along the wedge wall becomes simply

$$dx(q, \theta_s) = x_q(q, \theta_s)dq. \tag{5.4}$$

Using Eq. $(3.8)_1$ for the derivative x_q in the above, we have

$$dx(q, \theta_s) = Q(q, \theta_s)\psi_\theta(q, \theta_s)dq, \tag{5.5}$$

where

$$Q(q, \theta_s) = -\cos\theta_s \frac{1-\dfrac{\gamma+1}{\gamma-1}q^2}{q^2(1-q^2)^{\gamma/(\gamma-1)}}. \tag{5.6}$$

For practical purposes, the function $\psi_\theta(q, \theta_s)$ in the above can be easily expressed in the computational coordinate system (ξ, ω) in terms of ψ_ξ $(\xi = 1, \omega)$ only, since the other derivative ψ_ω $(\xi = 1, \omega)$ vanishes. In the hodograph polar, Eqs. $(5.3)_1$ and $(5.3)_2$ become

$$\begin{aligned} X_{\mathrm{I}} &= \int_{q=0}^{q_*} Q(q, \theta_{w_1}) \frac{\partial}{\partial\theta}\psi_{\mathrm{I}}(q, \theta_{w_1})dq \\ &= \frac{\cos\theta_{w_1}}{\cos\theta_{w_2}} \int_{q=q(D_2)}^{0} Q(q, -\theta_{w_2}) \frac{\partial}{\partial\theta}\psi_{\mathrm{I}}(q, -\theta_{w_2})dq, \\ X_{\mathrm{II}} &= \int_{q=0}^{q^*} Q(q, -\theta_{w_2}) \frac{\partial}{\partial\theta}\psi_{\mathrm{II}}(q, -\theta_{w_2})dq \\ &= \frac{\cos\theta_{w_2}}{\cos\theta_{w_1}} \int_{q=q(H_2)}^{0} Q(q, \theta_{w_1}) \frac{\partial}{\partial\theta}\psi_{\mathrm{II}}(q, \theta_{w_1})dq, \end{aligned} \tag{5.7}$$

where q^* is the sonic speed $((\gamma-1)/(\gamma+1))^{1/2}$, and $q(D_2)$ and $q(H_2)$ are the flow speeds at the downstream shock feet D_2 and H_2, respectively. The hodograph shock foot positions $q(D_2)$ and $q(H_2)$ are determined from the above two equations. The stream function of the form $\psi_i(q, \theta_s)$ in the above equations indicates that, if the subscript $i = \mathrm{I}$, it is the integral of Chaplygin's equation in the first Riemann sheet and, if $i = \mathrm{II}$, it is the stream function solved in the second Riemann sheet. The function $Q(q, \theta_s)$ in the integrands of Eqs. $(5.7)_1$ and $(5.7)_2$ has a second order singularity at $q = 0$ as is seen from Eqs. (5.6), and thus the integrals diverge near the integration limit $q = 0$. However, it is a removable singularity if the solution of the incompressible potential flow is used locally near the stagnation points. By the Schwarz–Christoffel transformation of the wedge to flat plates, we can show that the complex potential of the incompressible flow over a wedge of the inclination angle θ_s is

$$w_{\mathrm{inc}} = C_1 z^{\pi/(\pi-\theta_s)}: \ (z = re^{i\theta};\ w_{\mathrm{inc}} = \phi_{\mathrm{inc}} + i\psi_{\mathrm{inc}}). \tag{5.8}$$

The imaginary part of this equation is

$$\psi_{\text{inc}} = C_1 r^{\pi/(\pi-\theta_s)} \sin\left(\frac{\pi\theta}{\pi-\theta_s}\right). \tag{5.9}$$

Also the flow speed is given by

$$q_{\text{inc}}^2 = \frac{dw_{\text{inc}}}{dz} \cdot \overline{\frac{dw_{\text{inc}}}{dz}} \tag{5.10}$$

or

$$q_{\text{inc}} = C_2 r^{\theta_s/(\pi-\theta_s)}.$$

Using Eqs. (5.9) and (5.10), we obtain

$$\frac{d}{d\theta}\psi_{\text{inc}}\bigg|_{\theta=\theta_s} = C q_{\text{inc}}^{\pi/\theta_s} \tag{5.11}$$

which has, for a thin wedge of the small half wedge angle θ_s, a high order zero at the stagnation point. If this expression is used in Eqs. $(5.7)_1$ and $(5.7)_2$ in the small subinterval near the integration limit $q = 0$, i.e. in $0 \leqslant q = q_{\text{inc}} \leqslant \beta q^*$ where $\beta \lesssim 0.3$, then the terms in the equations become integrable. It is noted that the constant C in Eq. (5.11) is determined by matching the θ-derivative of the stream function of the incompressible flow with that of the compressible flow at the point of flow speed βq^*.

When Eqs. $(5.3)_1$ and $(5.3)_2$ or, more explicitly, Eqs. $(5.7)_1$ and $(5.7)_2$ are substituted into the closed body condition, Eq. (5.2), it is seen that the equation is not satisfied. This is due to the fact that in each of the two Riemann sheets the stream function, which is determined with the unknown multiplicative constant in Germain's term set to unity, is not appropriately amplified. For this reason $\psi_i(q, \theta_s)$ in Eqs. $(5.7)_1$ and $(5.7)_2$ may be replaced by $B_i \cdot \psi_i(q, \theta_s)$ where B_i, i = I and II, are the correction factors. From Eq. (5.2), with substitution of Eqs. $(5.7)_1$ and $(5.7)_2$, we can determine

$$B_{\text{I}} = \frac{\cos\theta_{w_1}\cos\alpha}{X_{\text{I}}(\cos\theta_{w_1}+\cos\theta_{w_2})},$$

$$B_{\text{II}} = \frac{\cos\theta_{w_2}\cos\alpha}{X_{\text{II}}(\cos\theta_{w_1}+\cos\theta_{w_2})}. \tag{5.12}$$

It may be noted that, given the downstream shock foot positions D_2 and H_2, the continuity conditions of the stream function and the velocity potential do not give unique upstream shock foot positions in the hodograph plane. This is due to the fact that the physical upstream shock foot points C_1 and G_1, which are singular, have their images on the epicycloid portions of the hodograph boundary. This means that the hodograph streamline and the equipotential line coincide with the epicycloid, a hodograph characteristic. To be able to isolate a single point as an upstream shock foot point, the velocity jump condition, Eq. (3.46), may be used.

To conclude this section it is pointed out that the imaginary part of the closed body condition, Eq. (5.1), yields no new information beyond that already provided by its real part.

5.2. Aerodynamic characteristics

The pressure coefficient C_p is defined by

$$C_p = \frac{\tilde{p}-\tilde{p}_\infty}{\frac{1}{2}\tilde{\varrho}_\infty \tilde{q}_\infty^2}. \tag{5.13}$$

In dimensionless form this becomes

$$C_p = \frac{\gamma-1}{\gamma}\frac{p-p_\infty}{\varrho_\infty q_\infty^2}, \tag{5.14}$$

where $p = \tilde{p}/\tilde{p}_0$ ($\tilde{p}_0$ is the stagnation pressure) is used, or

$$C_p(q) = \frac{\gamma-1}{\gamma}\frac{(1-q^2)^{\frac{\gamma}{\gamma-1}} - (1-q_\infty^2)^{\frac{\gamma}{\gamma-1}}}{q_\infty^2(1-q_\infty^2)^{1/(\gamma-1)}}. \tag{5.15}$$

Using the mapping equations, we have the following expressions:

$$\begin{aligned} dx(q,\theta_s) &= -\cos\theta_s \frac{1-\frac{\gamma+1}{\gamma-1}q^2}{q^2(1-q^2)^{\gamma/(\gamma-1)}}\frac{\partial}{\partial\theta}\psi_i(q,\theta_s)dq, \\ dy(q,\theta_s) &= -\sin\theta_s \frac{1-\frac{\gamma+1}{\gamma-1}q^2}{q^2(1-q^2)^{\gamma/(\gamma-1)}}\frac{\partial}{\partial\theta}\psi_i(q,\theta_s)dq, \end{aligned} \tag{5.16}$$

where i = I and II.

Then the pressure coefficient $C_p(x)$ or $C_p(y)$ is given parametrically by Eqs. (5.15), $(5.16)_1$ and $(5.16)_2$.

The drag coefficient is defined by

$$C_D = -\oint_{\text{Body}} C_p \mathbf{n}\cdot\mathbf{e}_x dl, \tag{5.17}$$

where $\mathbf{n}$ is an outward unit normal vector at a point on the airfoil surface, $\mathbf{e}_x$ is a unit vector pointing in the x-direction, and dl is an infinitesimal distance increment on the airfoil surface. For the double wedge, the above expression becomes

$$C_D = \int_{BC_1} C_p dy + \int_{D_2E} C_p dy - \int_{BG_1} C_p dy - \int_{H_2E} C_p dy. \tag{5.18}$$

On the other hand, the lift coefficient is

$$C_L = -\oint_{\text{Body}} C_p \mathbf{n}\cdot\mathbf{e}_y dl \tag{5.19}$$

which takes the following form for the double wedge:

$$C_L = -\int_{BC_1} C_p dx - \int_{D_2E} C_p dx + \int_{BG_1} C_p dx + \int_{H_2E} C_p dx. \tag{5.20}$$

5.3. Results and discussion

The problem described is solved for a double wedge of a wedge angle 9° in a high subsonic free stream of speed $q_\infty = 0.37$ ($M_\infty = 0.89$) and at angle of attack 1°. These figures are chosen so that the transonic potential flow model used in the theory is justified to the maximum extent.

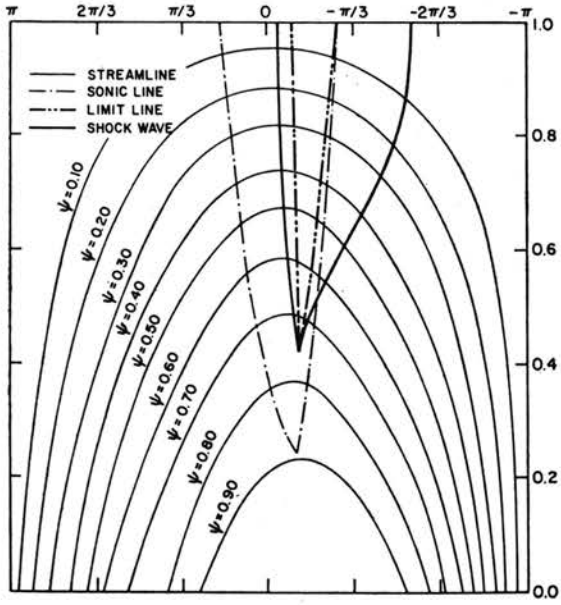

FIG. 13. Streamlines in the computational coordinate system (ξ, ω). The first Riemann surface.

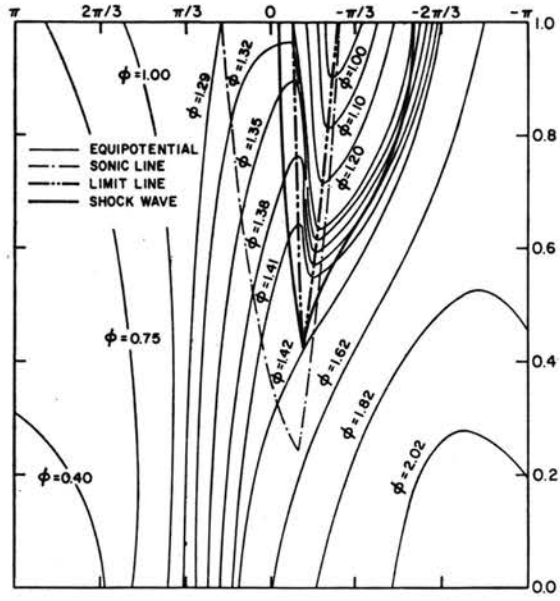

FIG. 14. Equipotentials in the computational coordinate system (ξ, ω). The first Riemann surface.

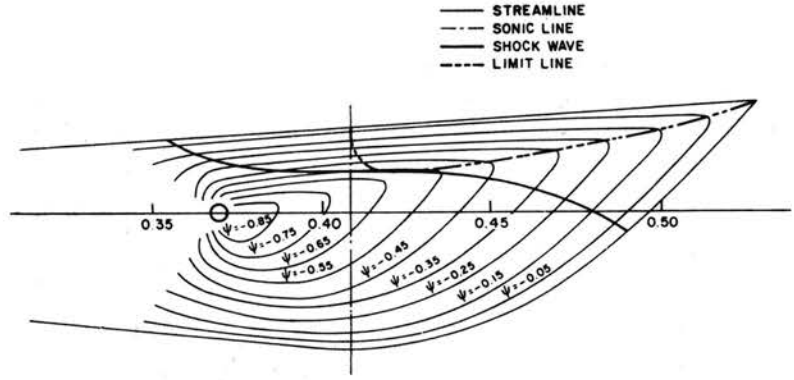

FIG. 15. Streamlines in the hodograph polar coordinate system (q, θ). The first Riemann surface.

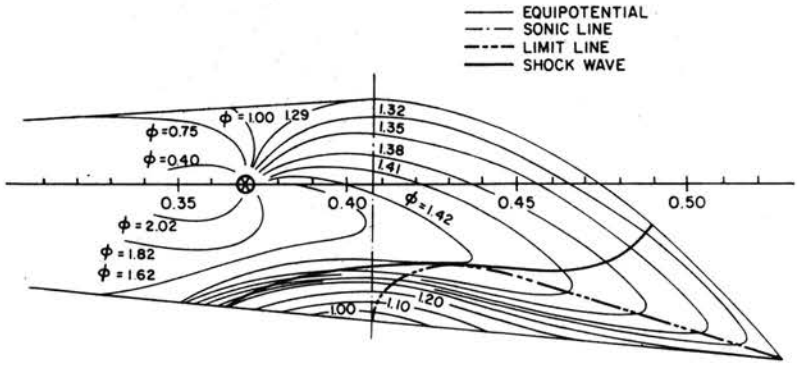

FIG. 16. Equipotentials in the hodograph polar coordinate system (q, θ). The first Riemann surface.

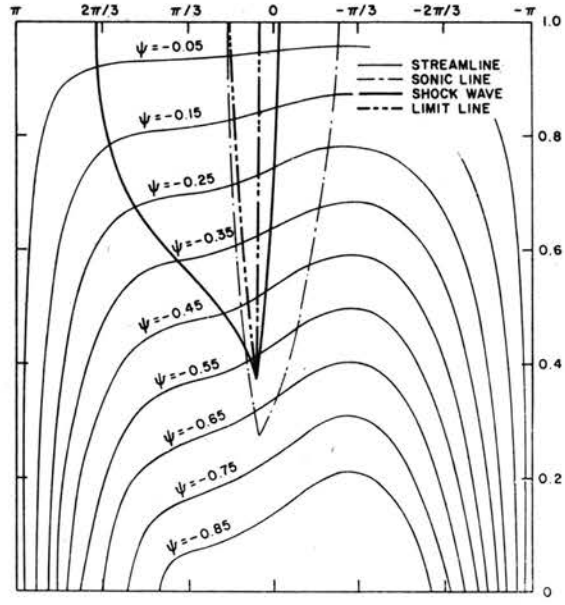

FIG. 17. Streamlines in the computational coordinate system (ξ, ω). The second Riemann surface.

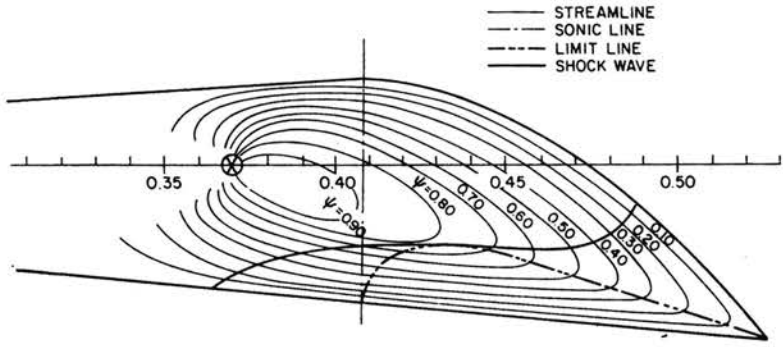

FIG. 18. Streamlines in the hodograph polar coordinate system (q, θ). The second Riemann surface.

Streamlines and equipotential lines are shown in Figs. 13, 14, 15 and 16 for the first Riemann surface. They clearly illustrate how the troublesome limit lines together with the adjacent, physically redundant regions could be excluded from the solution by a shock wave constructed with the fitting conditions, Eqs. (3.42), (3.44) and (3.45). In addition, Figs. 15 and 16 show how the hodograph shock wave osculates the limit line at the double point in the hodograph polar plane. Figures 17 and 18 represent the solution of Chaplygin's equation in the second Riemann surface. The shock wave in this case is based on the velocity jump condition across a shock, Eq. (3.46), in place of Eq. (3.45). The result is, indeed, not much different in quality from the previous one, the shock being of mild strength. The distribution of the flow speed q, Mach number, density and pressure coefficient C_p along the double wedge surface is presented in Figs. 19 and 20. The local lift coefficient in the chord direction is predicted in Fig. 21. The assumption made at the beginning of the present theory, that the leading stagnation point is attached at the nose of the double wedge is responsible for the unrealistic, vanishingly small local lift coefficient near $x = 0$. In reality, a shift of the stagnation point to a certain distance from the nose

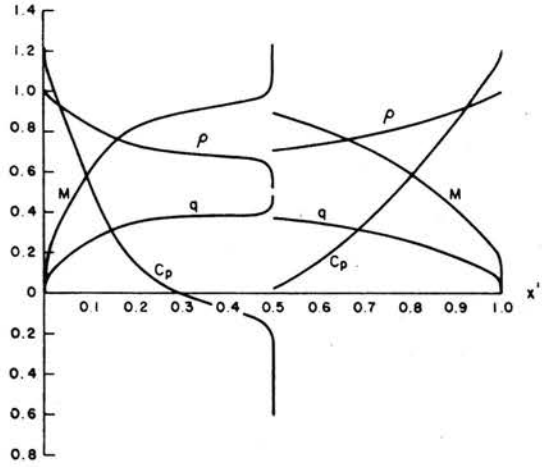

FIG. 19. Chordwise distribution of nondimensional quantities. Upper surface of the double wedge.

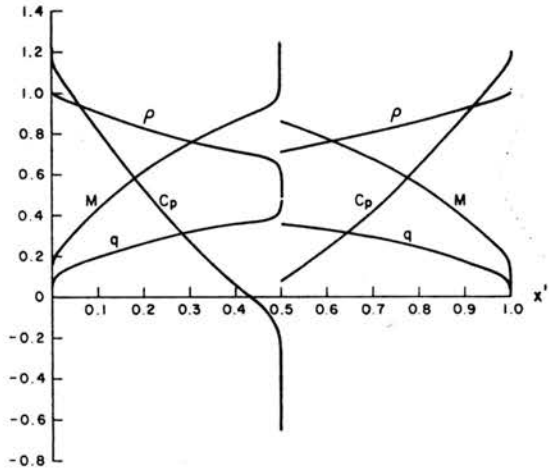

FIG. 20. Chordwise distribution of nondimensional quantities. Lower surface of the double wedge.

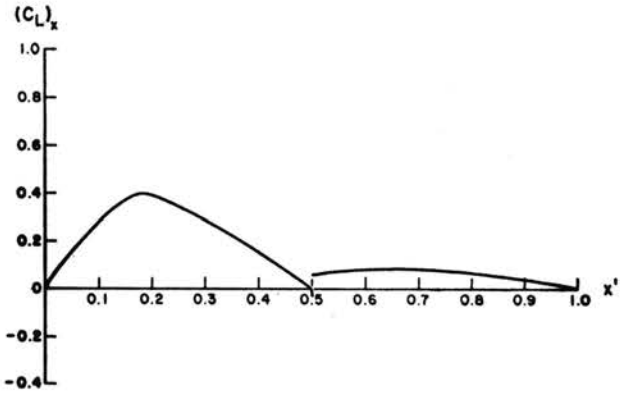

FIG. 21. Chordwise distribution of the local lift coeffcient of the double wedge.

on the lower forward surface of the double wedge will contribute to the production of a finite local lift at $x = 0$. On the other hand, the more realistic condition that the sonic speed is attained at the shoulder of the wedge surface leads to a more reasonable result near the mid-chord. The shock waves in the physical plane, Fig. 22, appear inside of the supersonic region near the tips, which is in agreement with TSUGE [38] and NOCILLA [32]. Tsuge, as a matter of fact, indicated that in general the end of the shock wave cannot reach the sonic point.

There has appeared no previous theory or experiments for comparison for the double wedge at an angle of attack in the range of high subsonic free stream speed. Unlike a streamlined airfoil, the existence of a small viscosity in the flow would cause a large adverse pressure gradient in the rear faces of the double wedge. The boundary layer-shock interaction will, in high probability, separate the flow downstream of the wedge shoulders, producing large experimental drag and less lift than calculated, and even dislocate the

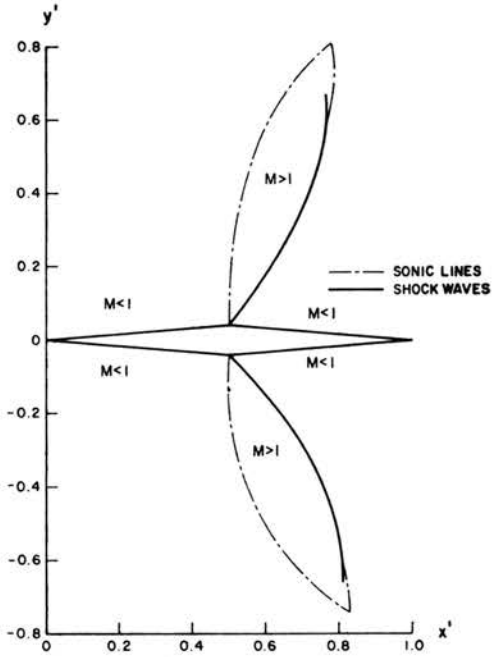

FIG. 22. Shock waves and sonic lines in the physical plane.

shock positions predicted by theory. Further, experimentally it is known to be difficult, due to the lack of resolution, to probe that part of the shock wave which is embedded in the supersonic region. It is remarkable that even in the theory the shock strength is so weak that the compression Mach wave becomes tangential to the shock wave toward its tip.

6. Conclusions

In the analysis of asymmetric supercritical transonic flow using hodograph equations, the double wedge has an inherent advantage, within the common approximation made in the literature, over the generalized airfoils: the boundary of the hodograph domain is known *a priori*. The theory presented in this report, however, provides an insight which extends, far beyond the flow past a double wedge, to the supercritical transonic flow in general. The combination of Telenin's method and the double sweep method has proven powerful in solving the Dirichlet type problems with mixed equations, for both the stream function and the velocity potential. Through shock fitting, limit lines which appear only in the transonic or supersonic potential flow are related directly to the experimental phenomena, the recompression shock waves. Fitted shocks, however, exhibit more sophisticated structure than experiment can provide: the end of the shock wave is embedded in the supersonic region. The lift coefficient would be more successfully predicted by the method if i) the accurate position of the leading stagnation point were given as a function of free

stream Mach number, wedge angle and angle of attack, ii) the flow behavior after a sharp turn at the forward vertex could be realistically incorporated into the solution, and iii) the hodograph far field conditions could be improved to a higher order of accuracy.

References

1. K. I. BABENKO, A. N. VOSKRESENSKY, A. N. LYUBIMOV and V. V. RUSANOV, *Three-dimensional flow of ideal gases around smooth bodies*, NASA TT F-380, 1963.
2. W. K. CHAN, *Cross flow separation on highly yawed cones in a supersonic stream*, Univ. of Calif., Ph. D. Thesis, Berkeley 1976.
3. J. J. CHATTOT, *Symmetrical flow past a double wedge at high subsonic Mach number*, J. Fluid Mech., **86**, 161–177, 1978.
4. P. I. CHUSHKIN, *Subsonic flow of a gas past ellipses and ellipsoids*, Vychisl. Matemat., **2**, 20–44, 1958.
5. J. W. CRAGGS, *The breakdown of the hodograph transformation for irrotational compressible fluid flow in two dimensions*, Proc. Camb. Phil. Soc., **44**, pp. 360–379, 1948.
6. J. C. CROWN, *Calculation of transonic flow over thick airfoils by integral method*, AIAA J., **6**, 413–423, March 1968.
7. A. A. DORODNITSYN, *Solution of mathematical and logical problems on high-speed digital computers*, Proc. Conf. Develop. Soviet Mach., Machines and Devices, Part 1, 44–52, VINITI, Moscow 1956.
8. H. W. EMMONS, *The numerical solution of compressible fluid flow problems*, NACA TN, 932. 1944.
9. H. W. EMMONS, *Flow of a compressible fluid past a symmetrical airfoil in a wind tunnnel and in free air*, NACA TN, 1746, 1948.
10. C. FERRARI and F. TRICOMI, *Transonic aerodynamics*, Academic Press. 1968.
11. C. A. J. FLETCHER, *Supersonic flow about cones at large angles of attack*, AIAA Journal, **13**, 1073–1078, 1975.
12. P. GERMAIN, *Problèmés mathématiques posés par l'application de la méthode de l'hodographe à l'etude des écouemlents transsoniques*, Symp. Transsonic., ed. K. OSWATITSCH, pp. 24–50, 1964.
13. S. M. GILINSKII, G. G. TELENIN and G. P. TINYAKOV, *A method of computing supersonic flow around blunt bodies, accompanied by a detached shock wave*, IZV. AN SSSR, Mekh. i Mash., 4, 9–28, NASA TT F-297, 1965.
14. M. B. GROSS, *Transsonic flow past an ellipse at high subsonic Mach numbers*, Univ. of Calif., Ph. D. Thesis, Berkeley 1975.
15. R. GROSSMAN and G. MORETTI, *Time-dependent computations of transonic flows*, AIAA Pap., 70–1322, October 1970.
16. G. GUDERLY and H. YOSHIHARA, *Two-dimensional unsymmetric flow patterns at Mach number*, J. Aero. Sci., **20**, 11, 757–768, 1953.
17. J. HADAMARD, *Lectures on Cauchy's problem*, Dover Publ., New York 1952.
18. M. HOLT (ed)., *Basic developments in fluid dynamics*, Part 1, Acad. Press. New York 1965.
19. M HOLT, *Numerical methods in fluid dynamics*, Springer Series in Computational Physics, Springer-Verlag, Berlin 1977.
20. M. HOLT and B. S. MASSON, *The calculation of high subsonic flow past bodies by the method of integral relations*, Proceedings of the Second International Conference on Numerical Methods in Fluid Dynamics, ed. M. HOLT, 8, Lect. Not. in Phys., pp. 207–214, Springer Verlag, Berlin 1971.
21. M. HOLT and D. E. NDEFO, *A numerical method for calculating steady unsymmetrical supersonic flow past cones*, J. Comp. Phys., **5**, 3, 463–486, 1970.
22. A. JAMESON, *Numerical computation of transonic flows with shock waves*, Symposium Transonicum II, ed. K. OSWATITSCH and D. RUES, Springer Verlag, pp. 384–414, Berlin 1976.
23. H. B. KELLER, *Numerical methods for two-point boundary value problems*, Blaisdell Publishing Co., Waltham, Mass., 1968.
24. G. H. KLOPFER, *Numerical solution of transsonic nozzle flows*, Univ. of Calif., Ph. D. Thesis, Berkeley 1975.

25. M. J. LIGHTHILL, *The hodograph transfomations*, Modern Developments in Fluid Dynamics-High Speed Flow, ed. L. HOWARTH, Vol. 1, Ch. VII, pp. 222–266, Oxford 1953.
26. R. MAGNUS and H. YOSHIHARA, *Inviscid transonic flow over airfoil*, AIAA Pap., 70–47, January 1970.
27. R. E. MELNIK and D. C. IVES, *Supercritical flows over two-dimensional airfoils by a multistrip method of integral relations*, Proceedings of the Second Intern. Conf. on Num. Methods in Fluid Dyn., ed. M. HOLT, 8, Lect. Not. in Phys., pp. 243–251, Springer Verlag, Berlin 1971.
28. L. M. MILNE-THOMPSON, *Theoretical hydrodynamics*, Macmillan Press, 1972.
29. E. M. MURMAN and J. D. COLE, *Calculation of plane steady transonic flows*, AIAA Pap., 70–188, January 1970.
30. E. M. MURMAN and J. A. KRUPP, *Solution of the transonic potential equation using a mixed finite difference scheme*, Proceedings of the Second Intern. Conf., on Num. Methods in Fluid Dyn., ed. M. HOLT, 8, Lect. Notes in Phys., pp. 199–206, Springer-Verlag, Berlin 1971.
31. J. NEWMAN, *Numerical solution of coupled, ordinary differential equations*, Industr. and Engineer., Chem., Fundamentals I, pp. 514–157, 1968.
32. S. NOCILLA, *Flussi transonici attorns a profili alari simmetrica con onda d'urto attaccata* ($M_\infty < 1$), Atti, Accad. Sci., Torino; Classe Sci. Fis. Mat. Nat., **92**, 282–307, 1958–1959.
33. M. J. D. POWELL, *An efficient method for finding the minimum of a function of several variables without calculating derivatives*, Comp. J., **7**, 155–162, 1964.
34. M. J. D. POWELL, *A method for minimizing the sum of squares of nonlinear function without calculating derivatives*, Comp. J., **7**, 303–307, 1965.
35. R. D. RICHTMYER and K. W. MORTON, *Difference methods for initial value problems*, Intersci. Publ., 2nd Ed., 1967.
36. J. L. STEGER and H. LOMAX, *Generalized relaxation methods applied to problems in transonic flow*, Proceeding of the Second Internat. Conf. of Numerical Meth. in Fluid Dyn., ed. M. HOLT, 8, Lect. Not. of Phys., Springer-Verlag, pp. 193–197, Berlin 1971.
37. T. C. TAI *Application of the method of integral relations to transonic airfoil problems*, AIAA Pap., 71–98, Jan. 1971.
38. S. TSUGE, *On the solution of the hodograph equation for the shock wave in locally supersonic zone*, T. Moriya Memorial Seminar for Aerodyn., Research Memorandum, 2, Japan 1959.
39. W. G. VINCENTI and C. B. WAGONER, *Theoretical study of the transonic lift of a double-wedge profile with detached bow wake*, NACA Rep., 1180, 1954.

DEPARTMENT OF MECHANICAL ENGINEERING
UNIVERSITY OF CALIFORNIA, BERKELEY, USA.

Received April 29, 1980.